Physics and modelling of hadronic interactions

MonteCarlo2000, Tutorials
Lisbon,22-26 October 2000

A. Ferrari

CERN, Geneva Switzerland (on leave from INFN-Milan)

Main steps of h-A interactions

h-A interactions can be schematically described as a sequence of the following steps:

- *Glauber-Gribov cascade and high energy collisions*
- *(Generalized)-IntraNuclear cascade*
- *Preequilibrium emission*
- *Evaporation/Fragmentation/Fission and final deexcitation*

Some of these steps can be missing if the energy of the projectile is low enough

h-A interactions

The approach to hadronic interaction modelling presented in the following is the one adopted by most state-of-the-art codes

In this "microscopic" approach, each step has sound physical basis. The performances are optimized comparing with particle production data at single interaction level. No tuning whatsoever on "integral" data, like calorimeter resolutions, thick target yields etc, is performed

The final predictions are obtained with minimal free parameters, fixed for all energies and target/projectile combinations

Results in complex cases as well as scaling laws and properties come out naturally from the underlying physical models. The basic conservation laws are fulfilled "a priori"

All the examples/results presented in the following have been obtained with FLUKA *and should be typical of codes adopting similar approaches*

Hadron-nucleon interaction models

Elastic, charge exchange and strangeness exchange reactions:

- Available phase-shift analysis and/or fits of experimental differential data
- At high energies, standard eikonal approximations are used

Particle production interactions: two kind of models

- Those based on "resonance" production and decays, which cover the energy range up to 3–5 GeV
- Those based on quark/parton string models, which provide reliable results up to several tens of TeV

Nucleon–nucleon cross sections

The p–p and p–n cross sections are rapidly increasing with decreasing energy

There is a factor three at the lowest energies between the n–p and the p–p cross sections, as expected on the basis of symmetry and isospin considerations

The total cross section for the two isospin components is given by:

$$\sigma_T^1 = \sigma_{pp}$$
$$\sigma_T^0 = 2\sigma_T^{np} - \sigma_T^{pp}$$

The same decomposition can be shown to apply for the elastic and the reaction cross sections too.

Nucleon–nucleon cross sections II

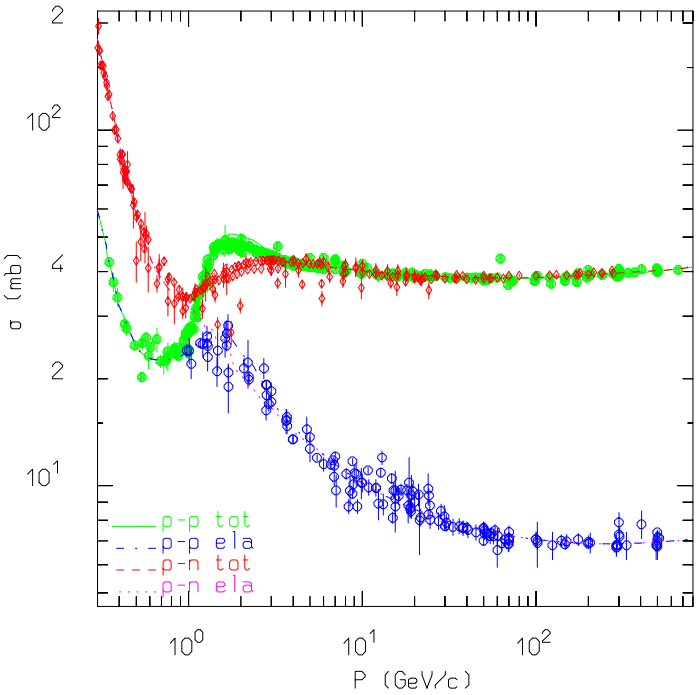

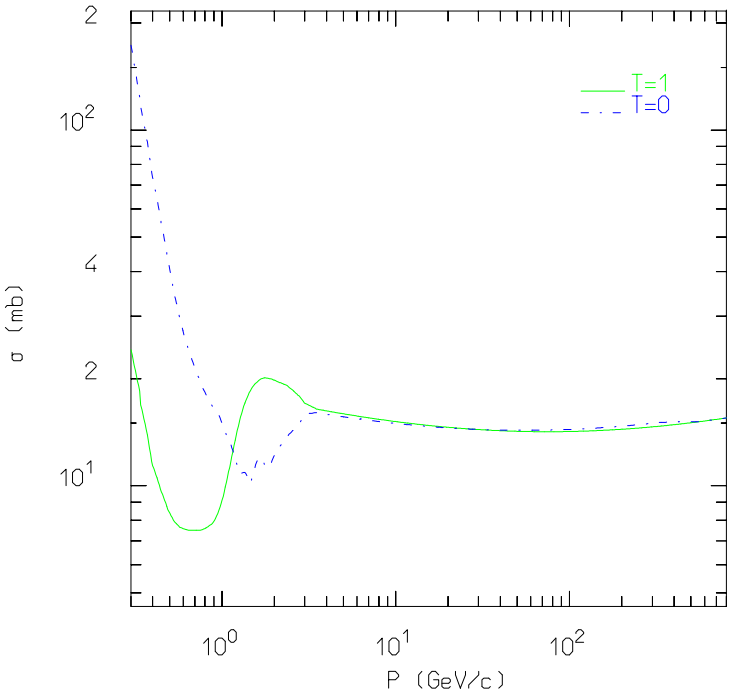

Total and elastic cross section for p–p and p–n scattering, together with experimental data (left), isospin decomposition in the T=0 and T=1 components (right)

π–nucleon cross sections

Pion isotopic spin: $T = 1 \rightarrow$ the three π charge states correspond to the three values of T_z. Thus, in the pion-nucleon system two values of T are allowed : $T = \frac{1}{2}$ and $T = \frac{3}{2}$, and two independent scattering amplitudes, $A_{\frac{1}{2}}$ and $A_{\frac{3}{2}}$, enter in the cross sections

From Clebsch-Gordan coefficients:

$$
\begin{aligned}
A\left(\pi^+ p \rightarrow \pi^+ p\right) &= A_{\frac{3}{2}} \\
A\left(\pi^- p \rightarrow \pi^- p\right) &= \frac{1}{3}\left(2A_{\frac{1}{2}} + A_{\frac{3}{2}}\right) \\
A\left(\pi^- p \rightarrow \pi^0 n\right) &= \frac{1}{3}\left(\sqrt{2}A_{\frac{3}{2}} - \sqrt{2}A_{\frac{1}{2}}\right) \\
A\left(\pi^0 p \rightarrow \pi^0 p\right) &= \frac{1}{3}\left(2A_{\frac{3}{2}} + A_{\frac{1}{2}}\right) \\
A\left(\pi^0 p \rightarrow \pi^+ n\right) &= A\left(\pi^- p \rightarrow \pi^0 n\right) \\
A\left(\pi^- n \rightarrow \pi^- n\right) &= A\left(\pi^+ p \rightarrow \pi^+ p\right) \\
A\left(\pi^+ n \rightarrow \pi^+ n\right) &= A\left(\pi^- p \rightarrow \pi^- p\right) \\
A\left(\pi^+ n \rightarrow \pi^0 p\right) &= A\left(\pi^- p \rightarrow \pi^0 n\right) \\
A\left(\pi^0 n \rightarrow \pi^0 n\right) &= A\left(\pi^0 p \rightarrow \pi^0 p\right) \\
A\left(\pi^0 n \rightarrow \pi^- p\right) &= A\left(\pi^0 p \rightarrow \pi^+ n\right)
\end{aligned}
$$

Using these relations all differential cross sections can be derived from the three measured ones:

$\sigma\left(\pi^+ p \rightarrow \pi^+ p\right)$, $\sigma\left(\pi^- p \rightarrow \pi^- p\right)$, $\sigma\left(\pi^- p \rightarrow \pi^0 n\right)$

π–nucleon cross sections II

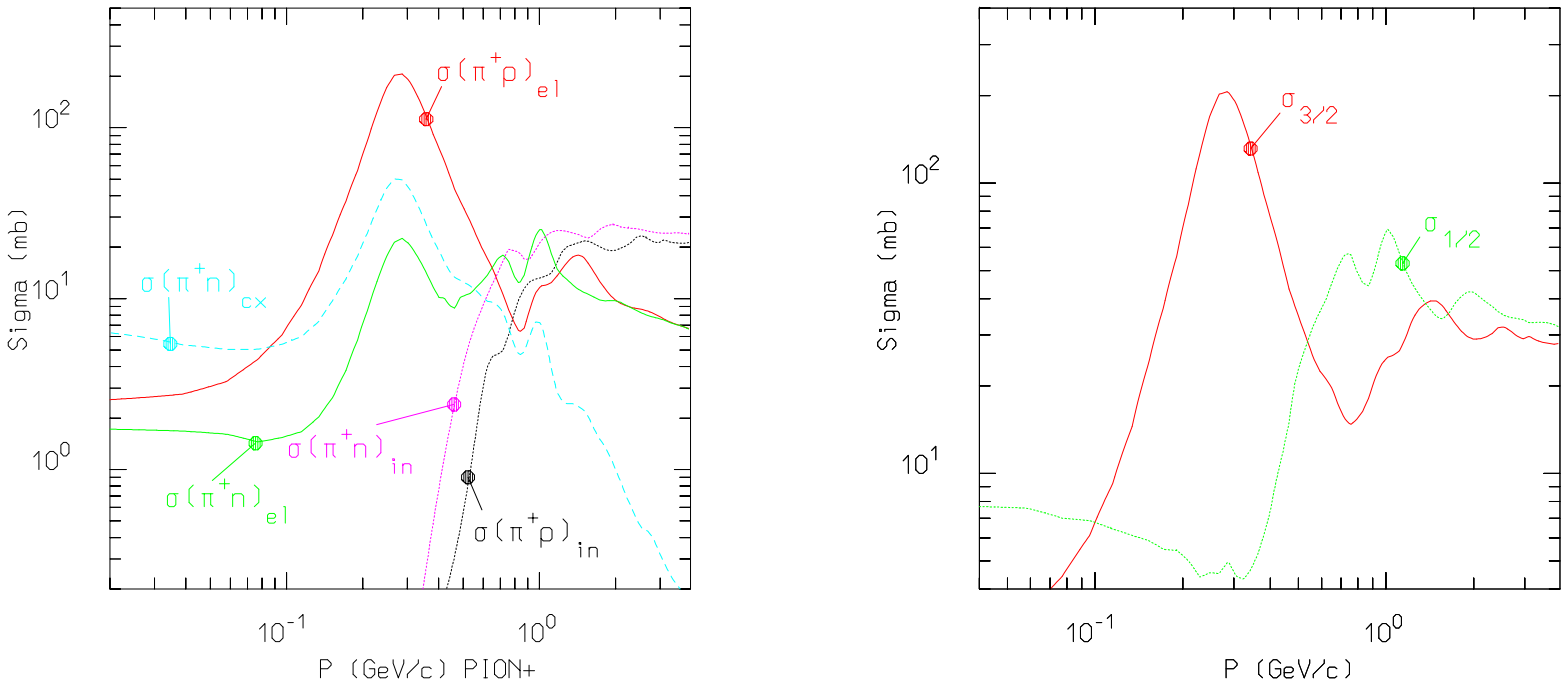

Elastic, chx and inel. cross sections for π–N scattering (left), isospin decomposition in the T=1/2 and T=3/2 components (right)

Nonelastic hN interactions at intermediate energies

- $N_1 + N_2 \to N_1' + N_2' + \pi$ threshold around 290 MeV, important above 700 MeV,
- $\pi + N \to \pi' + \pi'' + N'$ opens at 170 MeV.

Dominance of the Δ resonance and of the N^* resonances $\to$ reactions treated in the framework of the isobar model $\to$ all reactions proceed through an intermediate state containing at least one resonance.

$$
\begin{aligned}
N_1 + N_2 &\to N_1' + \Delta(1232) \to N_1' + N_2' + \pi \\
\pi + N &\to \Delta(1600) \to \pi' + \Delta(1232) \to \pi' + \pi'' + N' \\
N_1 + N_2 &\to \Delta_1(1232) + \Delta_2(1232) \to N_1' + \pi_1 + N_2' + \pi_2
\end{aligned}
$$

Resonance energies, widths, cross sections, branching ratios from data and conservation laws, whenever possible. Inferred from inclusive cross sections when needed

N-N nonelastic interactions at intermediate energies

Examples of N-N nonelastic interactions:

$$N_1 + N_2 \rightarrow N_1' + \Delta(1232) \rightarrow N_1' + N_2' + \pi$$
$$N_1 + N_2 \rightarrow N_1' + N^*(1440) \rightarrow N_1' + N_2' + \pi$$

where the $N^*(1440)$ is a $\mathrm{T}(\mathrm{J}^P)=\frac{1}{2}\left(\frac{1}{2}^+\right)$ baryon resonance with sizeable decay channels into one or two pions plus one nucleon.

π-N Nonelastic interactions at intermediate energies

Possibility of direct production of s-channel resonances (that is π N going into one resonance, like the Δ), which are not possible in the N N system since no dibaryon resonance has ever been discovered.

Examples:

$$\begin{aligned}
\pi + N &\rightarrow N^*(1440) \rightarrow \rho(770) + N' \rightarrow \pi' + \pi'' + N' \\
\pi + N &\rightarrow \Delta(1600) \rightarrow \pi' + \Delta(1232) \rightarrow \pi' + \pi'' + N' \\
\pi + N &\rightarrow \rho(770) + N' \rightarrow \pi' + \pi'' + N' \\
\pi + N &\rightarrow \pi' + \Delta(1232) \rightarrow \pi' + \pi'' + N'
\end{aligned}$$

where the first two reactions are examples of s-channel direct resonance production. $\rho(770)$ is a T(J^P)=1 (1^+) meson resonance with 100% decay branching into $\pi\pi$.

Multiple pion production at intermediate energies

The isobar model easily accommodates multiple pion production, for example allowing the presence of more than one resonance in the intermediate state (double pion production opens already at 600 MeV in nucleon-nucleon reactions, and at about 350 MeV in pion-nucleon ones).

Examples of two pion production for $N - N$:

$$N_1 + N_2 \rightarrow \Delta_1(1232) + \Delta_2(1232) \rightarrow N_1' + \pi_1 + N_2' + \pi_2$$
$$N_1 + N_2 \rightarrow N_1' + N^*(1440) \rightarrow N_1' + \pi_1 + \Delta(1232) \rightarrow N_1' + \pi_1 + N_2' + \pi_2$$
$$N_1 + N_2 \rightarrow N_1' + \Delta(1600) \rightarrow N_1' + \pi_1 + N^*(1440) \rightarrow N_1' + \pi_1 + N_2' + \pi_2$$

and for pion-nucleon:

$$\begin{aligned} \pi + N &\rightarrow \Delta(1600) \rightarrow \pi' + N^*(1440) \rightarrow \pi' + \pi'' + \Delta(1232) \\ &\rightarrow \pi' + \pi'' + \pi''' + N' \\ \pi + N &\rightarrow \omega(782) + N' \rightarrow \pi' + \pi'' + \pi''' + N' \\ \pi + N &\rightarrow \rho(770) + \Delta(1232) \rightarrow \pi' + \pi''' + \pi'' + N' \end{aligned}$$

Pion production at intermediate energies: summary

Summarizing, all reactions can be thought to proceed through channels like:

$$h + N \rightarrow X \rightarrow x_1 + ... + x_n \quad (1)$$

$$h + N \rightarrow X + Y \rightarrow x_1 + ... + x_n + y_1 + ... + y_m \quad (2)$$

where X and Y can be real resonances, or stable particles (n, p, π) directly.

Resonances which appear in the intermediate states can be treated as real particles, that is, in a MonteCarlo code they can be transported and then transformed into secondaries according to their lifetimes and decay branching ratios. Reactions described by eq. 1 are examples of s-channel direct resonance production $\rightarrow$ **bumps** in the corresponding isospin cross section around the centre-of-mass energy corresponding to the resonance mass.

The reactions proceeding like in 2, due to the presence of two particles in the intermediate state with the associated extra degree of freedom of their relative motion, do not exhibit a resonant behaviour, but rather a relatively fast increase starting from a centre-of-mass energy, $\sqrt{s} \approx M_X + M_Y$, followed by a smooth behaviour. $N\ N$ reactions are all of this latter type and therefore no resonant structure can be find in $N\ N$ cross sections.

Inelastic hN at high energies: (DPM, QGSM, ...)

- Problem: "soft" interactions $\rightarrow$ no perturbation theory.
- Solution : Interacting strings (quarks held together by the gluon-gluon interaction into the form of a string)
- Interactions treated in the Reggeon-Pomeron framework
- At sufficiently high energies the leading term corresponds to a Pomeron (IP) exchange (a closed string exchange)
- Each colliding hadron splits into two colored partons $\rightarrow$ combination into two color neutral chains $\rightarrow$ two back-to-back jets
- Physical particle exchange produce single chains at low energies
- Higher order contributions with multi-Pomeron exchanges important at $E_{lab} \geq$ 1 TeV

DPM and hadronization

from DPM:

- Number of chains
- Chain composition
- Chain energies and momenta
- Diffractive events

Almost No Freedom

Chain hadronization

- Assumes chain universality
- Fragmentation functions from hard processes and e^+e^-
- Transverse momentum from uncertainty considerations
- Mass effects at low energies

The same functions and (few) parameters for all reactions and energies

DPM: chain examples

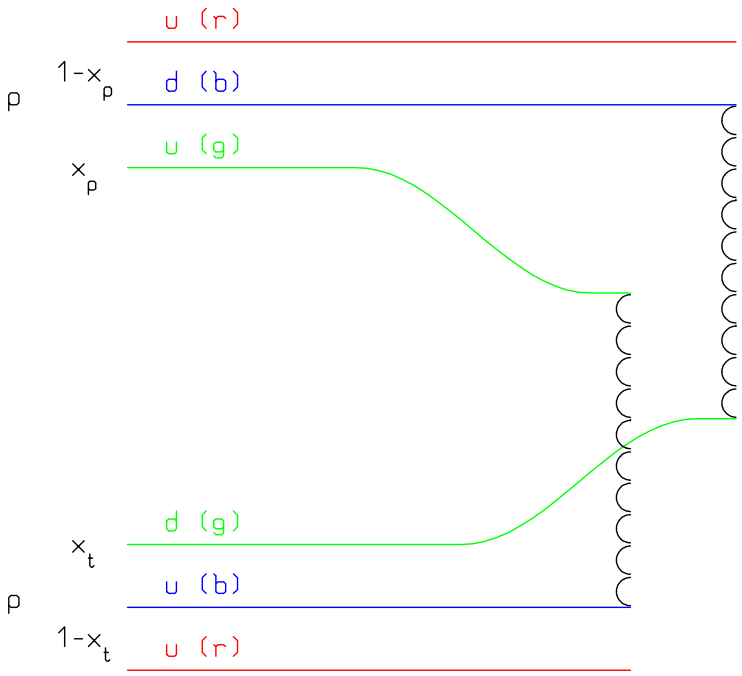

Leading two-chain diagram in DPM for $p-p$ scattering. The color (red, blue, and green) and quark combination shown in the figure is just one of the allowed possibilities

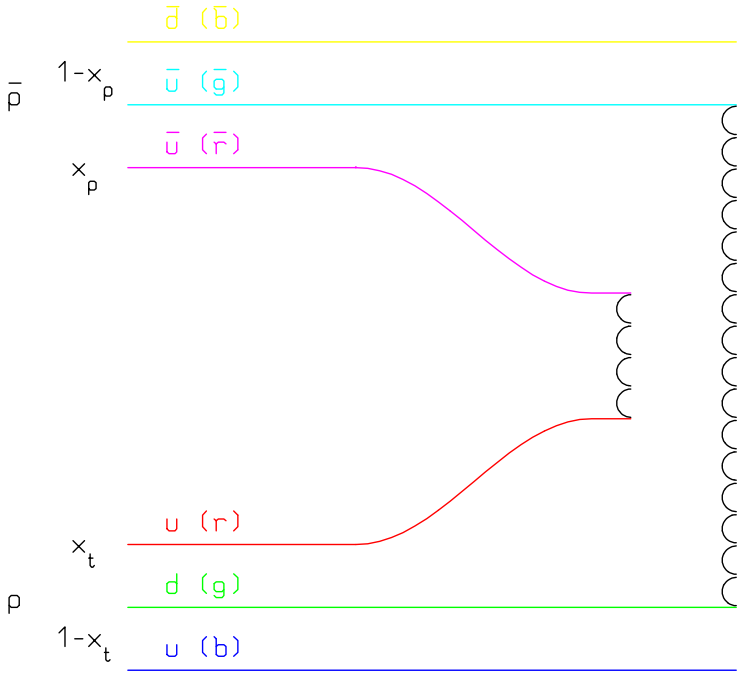

Leading two-chain diagram in DPM for $\bar{p}-p$ scattering. The color (red, blue, and green) and quark combination shown in the figure is just one of the allowed possibilities

DPM: chain examples II

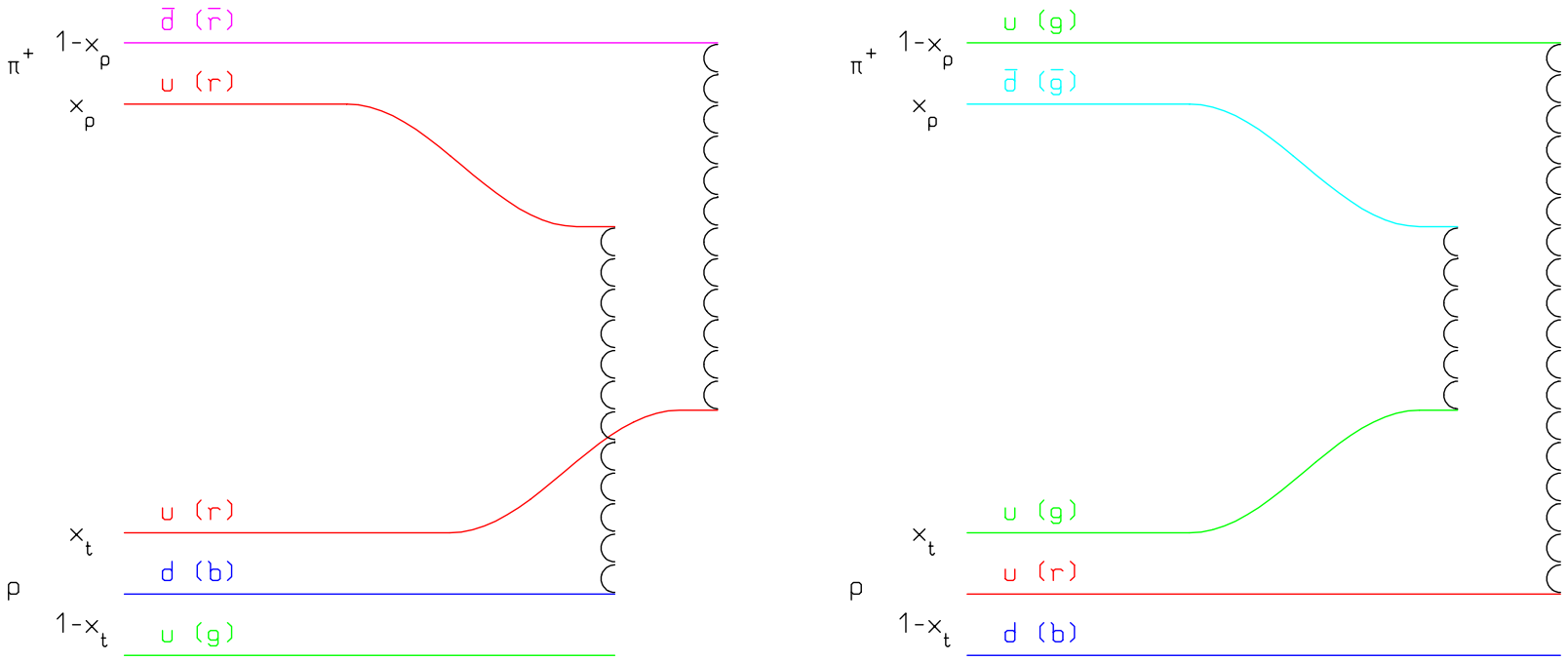

Leading two-chain diagrams in DPM for $\pi^+ - p$ scattering. The color (red, blue, and green) and quark combination shown in each figure is just one of the allowed possibilities

Nonelastic hN at high E :(π^+ p), 7-22 GeV

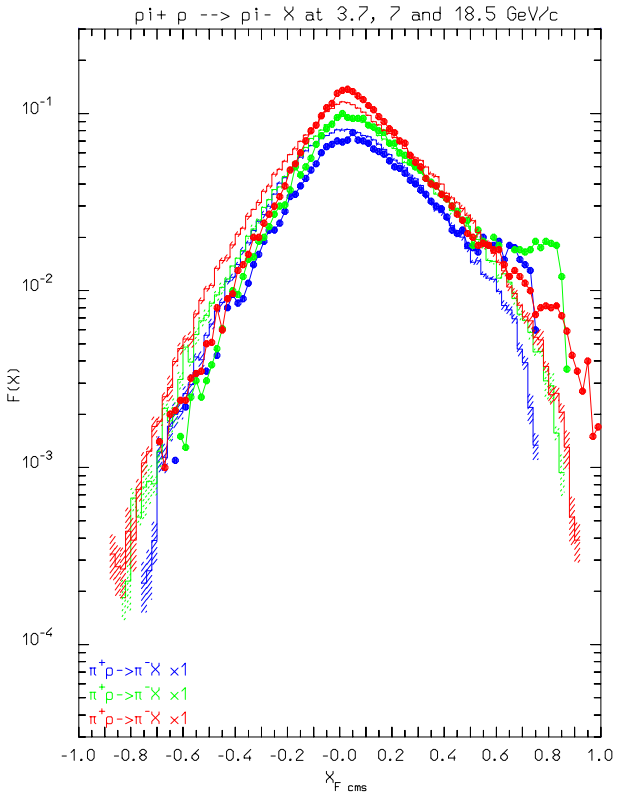

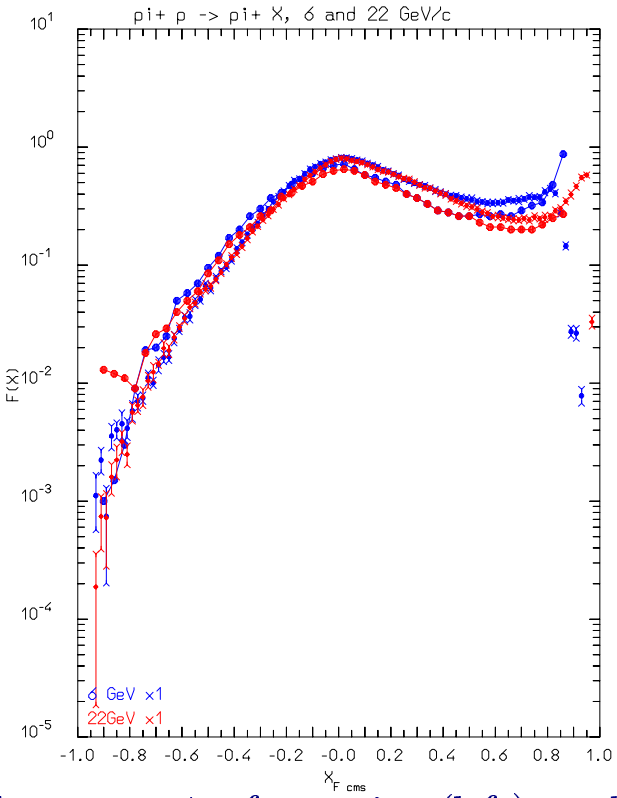

Invariant cross section spectra, as a function of Feynman x_F^* of negative (left), and positive (right) pions emitted for π^+ on protons at various momenta. Data from M.E Law et al. LBL80 (1972).

Nonelastic hN high E: (K^-p) , (π^-p) 10-16 GeV, p_T

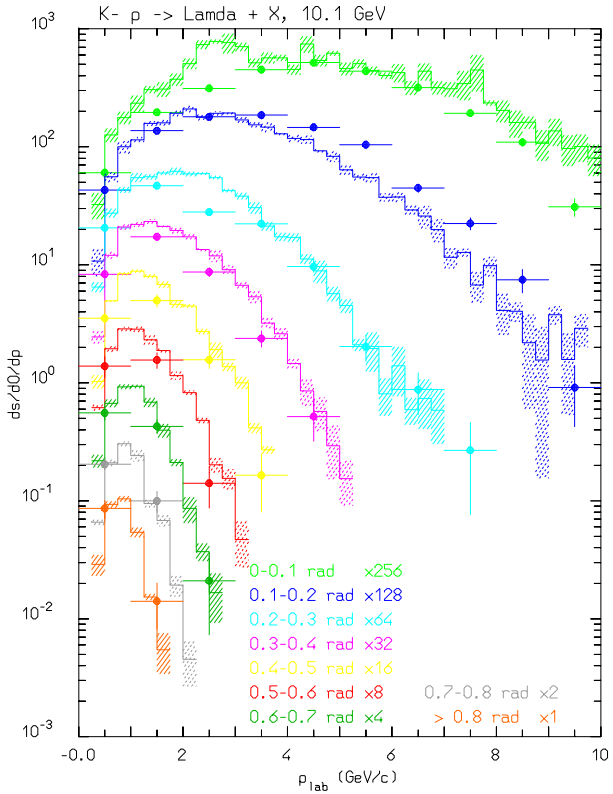

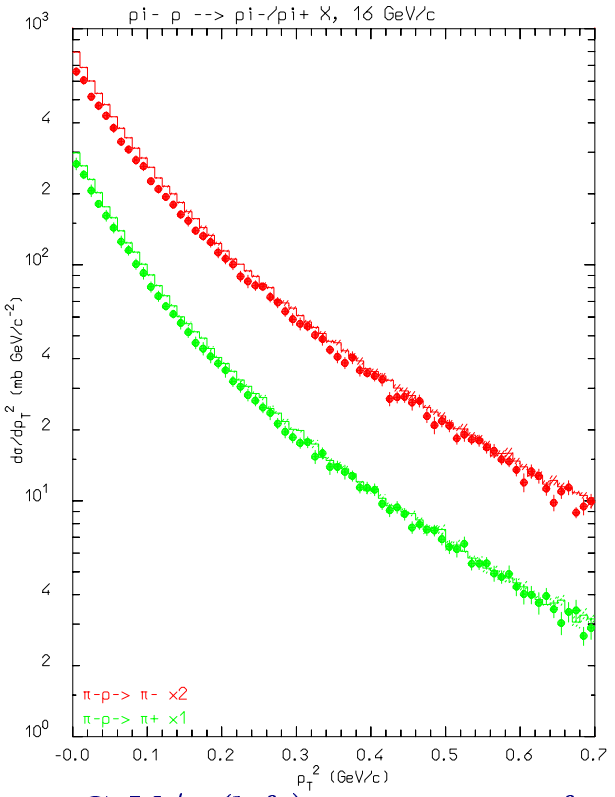

Double differential cross section for $K^-p \to \Lambda X$ at 10 GeV/c (left), p_T spectra of π^+ and π^- produced by 16 GeV/c π^- incident on an hydrogen target. Data from M.E Law et al. LBL80 (1972).

Nonelastic hN high E: (π^+ p) 250GeV, x_F and p_t

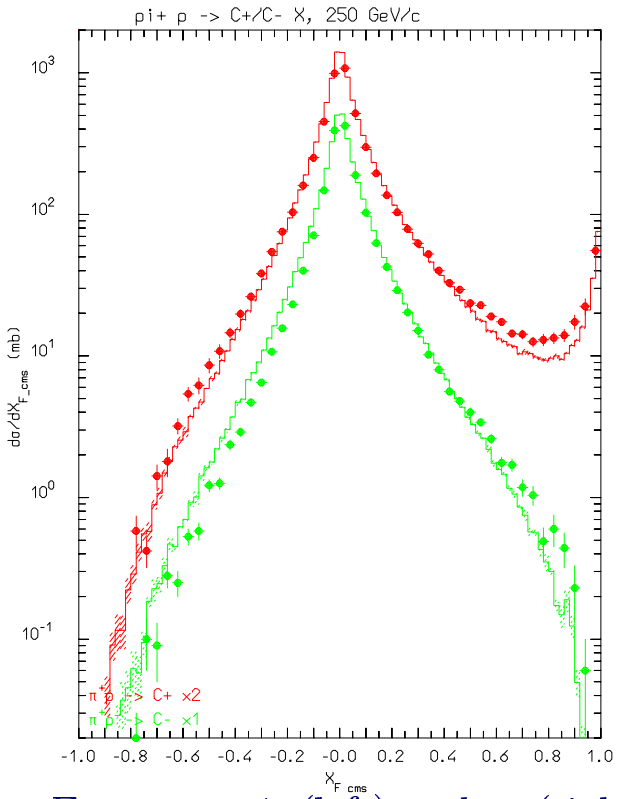

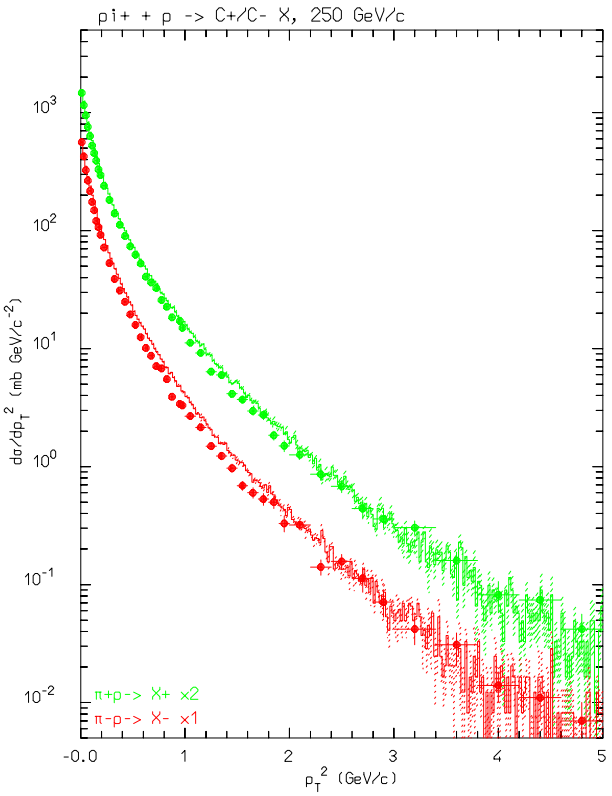

Feynman x_F^* (left) and p_t (right) spectra of positive particles and π^- produced by 250 GeV/c π^+ incident on an hydrogen target. Exp. data (symbols) have been taken from M. Adamus et al. ZPC39, 311 (1988).

Cross sections: examples

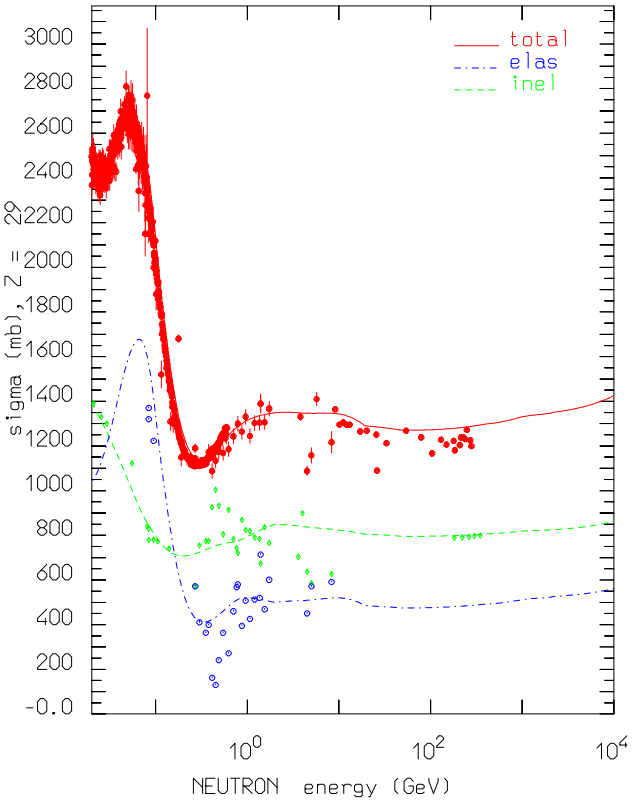

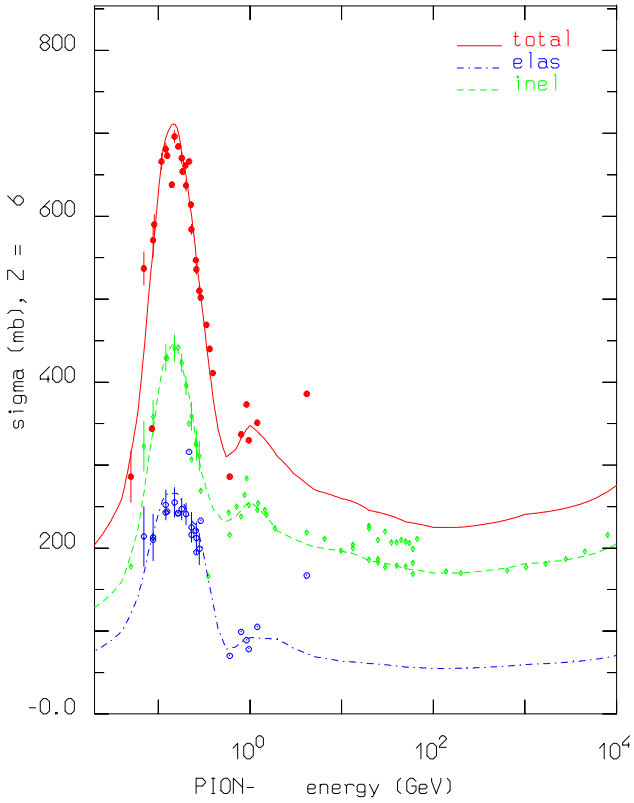

MonteCarlo (FLUKA) and experimental cross sections for neutrons on copper (left) and negative pions on carbon (right)

Cross sections: examples II

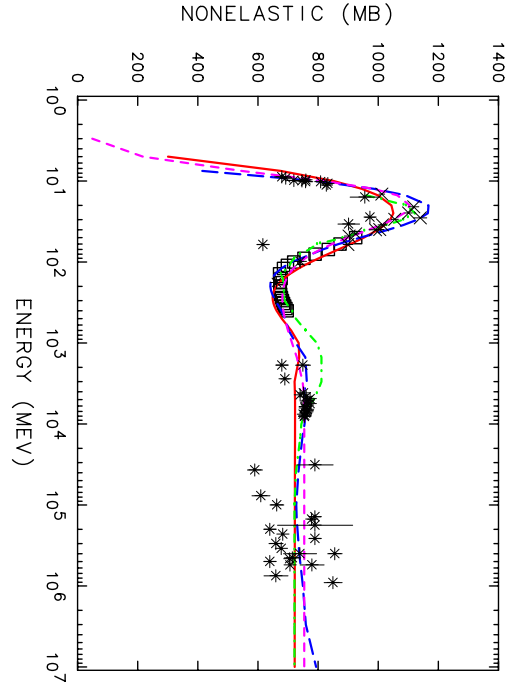

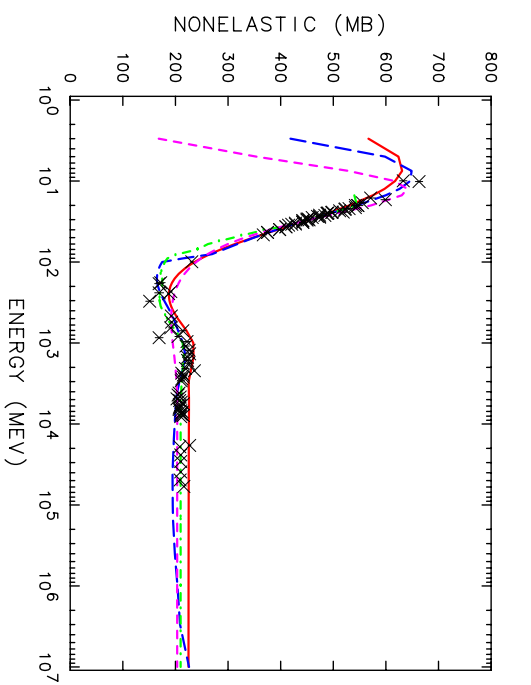

(Generalized) IntraNuclear Cascade basic assumptions

1. Primary and secondary particles moving in the nuclear medium
2. *Target nucleons motion and nuclear well according to the Fermi gas model*
3. Interaction probability from σ_{free} + Fermi motion $\times$ $\rho(r)$ + exceptions (ex. π)
4. *Glauber cascade at high energies*
5. Classical trajectories $(+)$ nuclear mean potential (*resonant for π's!!*)
6. Curvature from nuclear potential $\rightarrow$ refraction and reflection.
7. Interactions are incoherent and uncorrelated
8. Interactions in projectile–target nucleon CMS $\rightarrow$ Lorentz boosts
9. *Multibody absorption for π, μ^-, K^-*
10. *Quantum effects (Pauli, formation zone, correlations...)*
11. *Exact conservation of energy, momenta and all additive quantum numbers,including nuclear recoil*

h-A at high energies: the Glauber Cascade

Elastic, Quasi-elastic and Absorption hA cross sections derived from Free hadron-Nucleon cross section + Nuclear ground state ONLY.

Inelastic interaction $\equiv$ multiple interaction with ν target nucleons, with binomial distribution (at a given impact parameter, b):

$$P_{r\ \nu}(b) \equiv \left(\begin{array}{c} A \\ \nu \end{array} \right) P_r^{\nu}(b) \left[1 - P_r(b)\right]^{A-\nu}$$

where $P_r(b) \equiv \sigma_{hN\ r} T_r(b)$, and $T_r(b)$= profile function *(folding of nuclear density and scattering profiles along the path).*

On average :

$$< \nu > \ = \ \frac{Z\sigma_{hp\ r} + N\sigma_{hn\ r}}{\sigma_{hA\ abs}}$$

$$\sigma_{hA\ abs}(s) \ = \ \int \mathrm{d}^2\vec{b} \left[1 - \left(1 - \sigma_{hN\ r}(s) T_r(b)\right)^A\right]$$

h-A at high energies: Glauber-Gribov

Glauber-Gribov = diagram interpretation of the Glauber cascade

Used by QGSM/DPM/... for modelling Multiple Collisions

Interaction with ν target nucleons

$\Downarrow$

2ν chains, out of which

2 chains struck between the projectile and target valence (di)quarks,

$2(\nu-1)$ chains between projectile sea $q-\bar{q}$ and target valence (di)quarks.

No freedom, except in the treatment of mass effects at low energies.

Fermi motion included $\rightarrow$ smearing of p_T distributions

(G)INC follows

Nonelastic hA interactions at high energies: examples

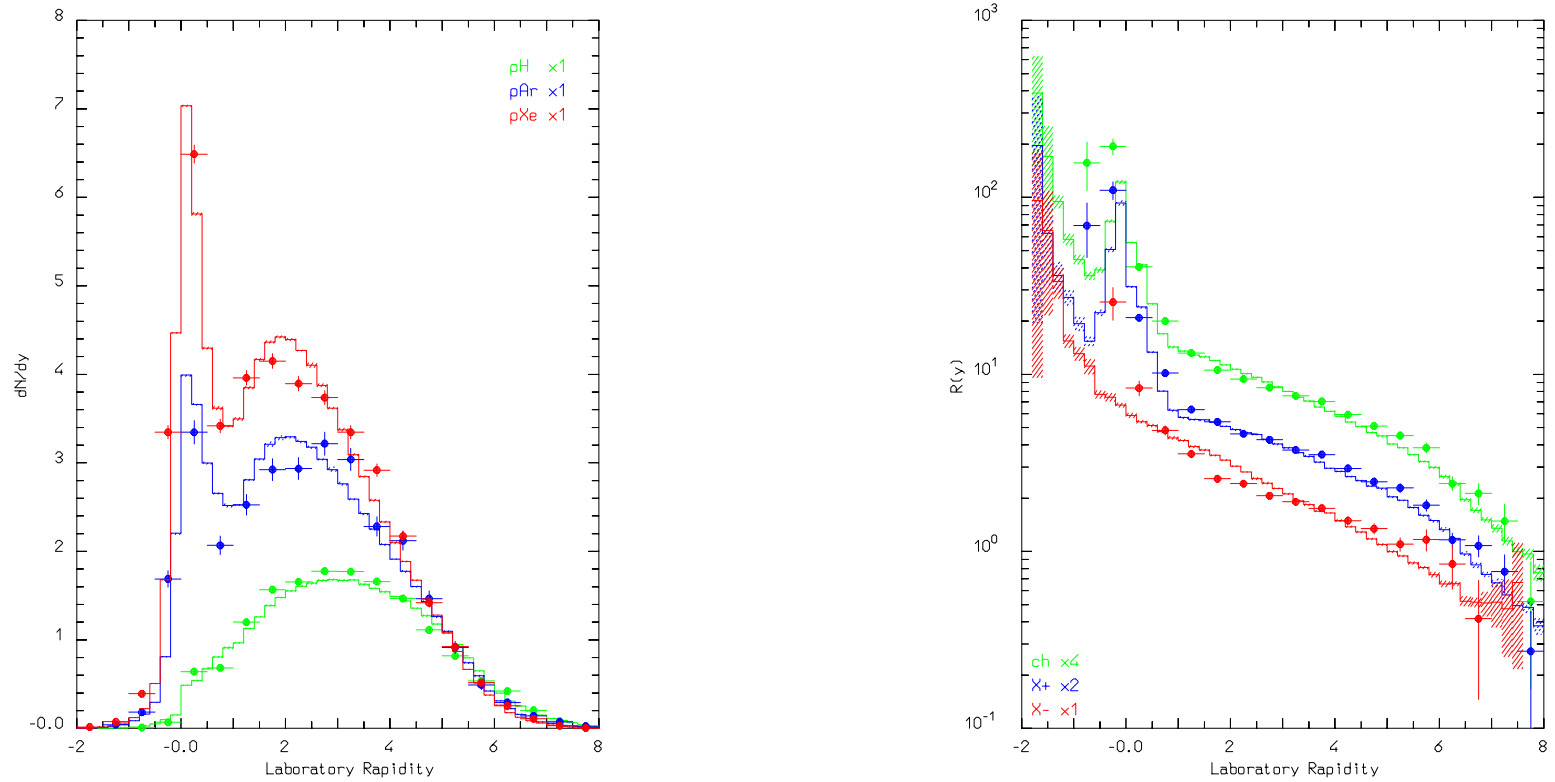

Rapidity distribution of charged particles produced in 200 GeV proton collisions on Hydrogen, Argon, and Xenon target (left) and ratio of rapidity distribution of charged, positive, and negative particles produced in 200 GeV proton collisions on Xenon and Hydrogen (right). Data from C. De Marzo et al., PRD26, 1019 (1982).

Nonelastic hA interactions at high energies: examples

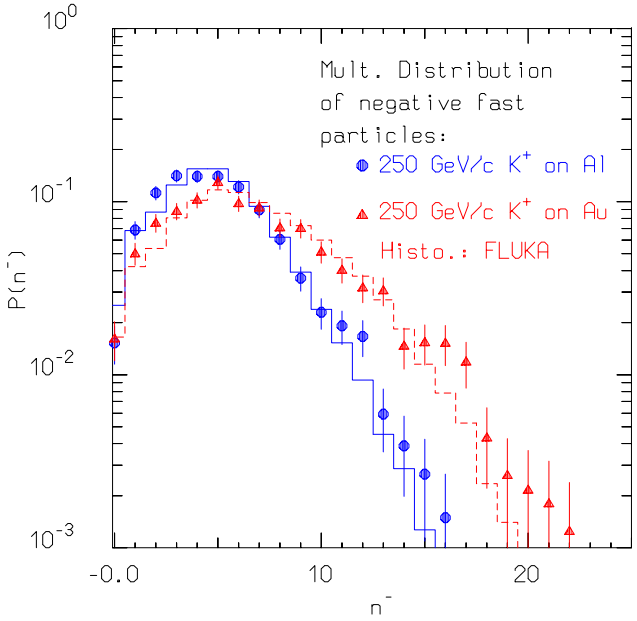

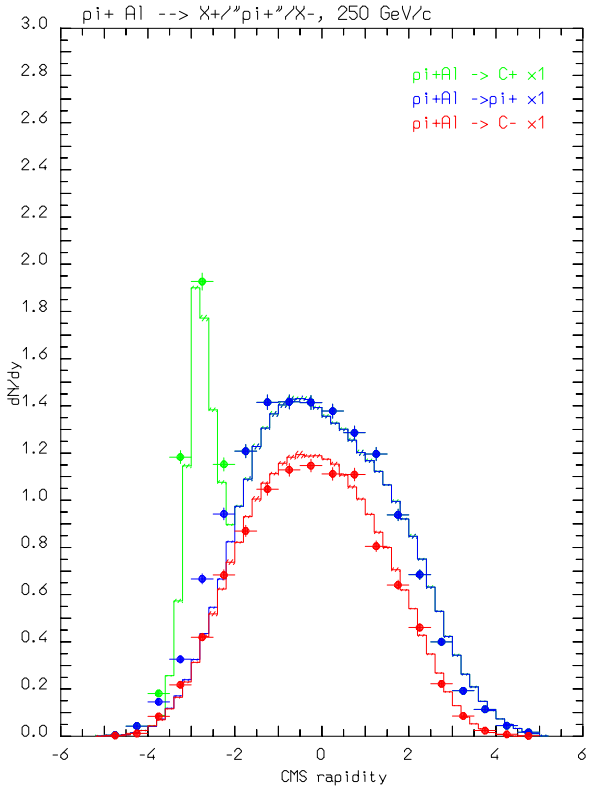

Multiplicity distribution of negative shower particles for 250 GeV/c K^+ on Aluminium and Gold targets (left), and rapidity distribution of positive, negative, and "π^+" particle for 250 GeV/c π^+ on Aluminium (right). Data from I.V. Ajinenko et al. ZPC42 377 (1989) and N.M. Agababyan et al. ZPC50 361 (1991).

h-A interactions: the multiplicity distribution vs the Glauber cascade

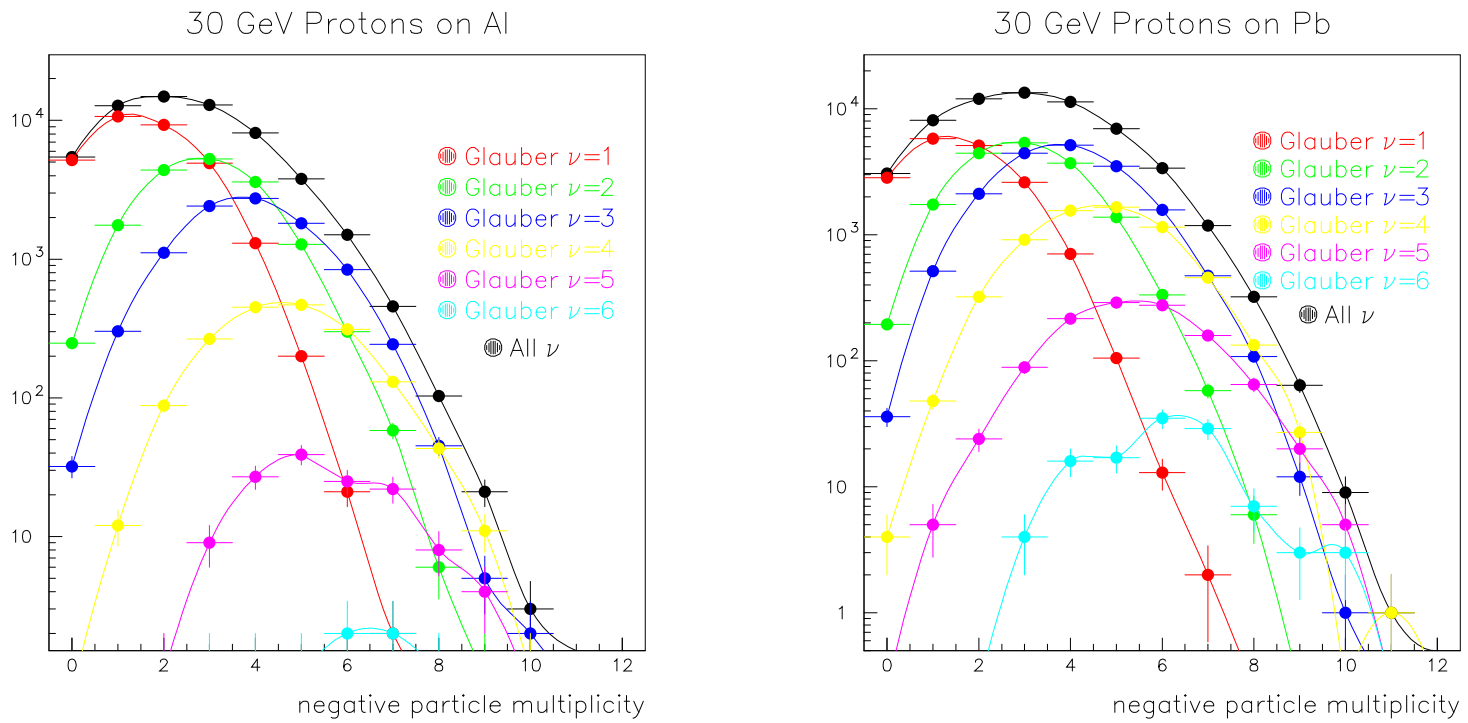

Negative particle multiplicity distribution for 30 GeV protons on Al (left) and Pb (right), total and for given numbers of primary collisions

Quantistic effects in (G)INC

1. *Pauli blocking,*
2. *Formation time (inelastic),*
3. *Coherence length ((quasi)-elastic and charge exchange),*
4. *Nucleon antisymmetrization,*
5. Hard core nucleon correlations

Nucleon Fermi Motion

Fermi gas model: nucleons as non-interacting fermions constrained in a cubic box of linear dimension a.

The nucleon wave functions are those of a free-particle with the condition $\Psi(x,y,z)=0$ at the nuclear boundary, thus with constraints on the three components of the momentum:

$$K_x a = n_x \pi \quad K_y a = n_y \pi \quad K_z a = n_z \pi$$

where the n's are positive integers. Each set of integers defines a solution of the Schrödinger equation with energy given by:

$$\begin{aligned} E(n_x,n_y,n_z) &= \frac{\hbar^2}{2M}|K|^2 \\ |K|^2 &= (K_x^2+K_y^2+K_z^2) \end{aligned}$$

Nucleons must obey the Pauli principle, → for each set of n's, → for a given momentum state, there can be at most four nucleons, two protons and two neutrons, each pair with opposite spin

Nucleon Fermi Motion II

Each solution occupies a box in momentum space given by $\left(\frac{\pi}{a}\right)^3$; thus the number of states with momentum comprised between K and $K+dK$ is given by the volume of the spherical shell of radius K and thickness dK divided by the volume occupied by each single solution, and divided again by eight since we consider only positive values of n_x, n_y, n_z:

$$\begin{aligned} \mathrm{d}N &= \frac{|K|^2}{2\pi^2}\Omega dK, \quad \Omega = a^3 \\ \mathrm{d}N &= \frac{\Omega m}{2\pi^2\hbar^3}\sqrt{2mE}\mathrm{d}E \end{aligned}$$

Thus, the total number of states with momentum smaller than $|K_F|$ is given by:

$$n(K_F) = \frac{4\pi}{3}\frac{K_F^3}{8(\pi/a)^3}$$

If we take N=Z=A/2, and place 4 nucleons on each level, we get:

$$A = \frac{2\Omega}{3\pi^2}K_F^3$$

$\Rightarrow$ *the momentum of the highest occupied state depends only on the nuclear density* $\rho = A/\Omega$*:*

$$\rho = \frac{2}{3\pi^2}K_F^3$$

Nucleon Fermi Motion III

The observed density of nuclei, $\rho = 1.7 \times 10^{38}$ nucleons/cm^3, implies:

$$K_F = 1.36 \text{ fm}^{-1}$$
$$E_F = 38 \text{ MeV}$$

These are called the **Fermi momentum** *and* **Fermi Energy**

In nuclei with $N \neq Z$, two different values of the Fermi energy can be defined:

$$\rho_n = \frac{N}{A}\rho = \frac{(K_F^n)^3}{3\pi^2}$$
$$\rho_p = \frac{Z}{A}\rho = \frac{(K_F^p)^3}{3\pi^2}$$

The so defined Fermi energies are obviously kinetic energies, that is energies counted from the bottom of a potential well that in this model must be input from outside. This gives an average potential depth of about 38+8=46 MeV. The Fermi energy can be made radius-dependent in a straightforward way, through the so called *local density approximation*:

$$\rho(r) = \frac{2}{3\pi^2}K_F^3(r)$$

Nucleon correlation function

Correlation function: it can be computed within the Fermi-gas model

Due to the antisymmetrization of the fermion's wave function, given a nucleon in a position $\vec{r}$ *in a nucleus with density* ρ_0*, the probability of finding another like nucleon in a position* $\vec{r}\,'$ *is decreased for small values of the distance* $r = |\vec{r} - \vec{r}\,'|$ *by a factor*

$$g(x) \;=\; 1 - \frac{1}{2}\left[\frac{3}{x^2}\left(\frac{\sin x}{x} - \cos x\right)\right]^2$$

where $x = K_F \cdot r$*, and the factor* $\frac{1}{2}$ *in front of the parenthesis accounts for the two possible spin orientations.*

Formation Zone

Naively: "materialization" time. Qualitative estimate: in the frame where $p_{\|} = 0$

$$\bar{t} \;=\; \Delta t \approx \frac{\hbar}{E_T} = \frac{\hbar}{\sqrt{p_T^2 + M^2}}$$

particle proper time

$$\tau \;=\; \frac{M}{E_T}\bar{t} = \frac{\hbar M}{p_T^2 + M^2}$$

Going to lab system

$$t_{lab} \;=\; \frac{E_{lab}}{E_T}\bar{t} = \frac{E_{lab}}{M}\tau = \frac{\hbar E_{lab}}{p_T^2 + M^2}$$

As a function of particle rapidity y

$$t_{lab} = \bar{t}\cosh y = \frac{\hbar}{\sqrt{p_T^2 + M^2}}\cosh y$$

Condition for possible reinteraction inside a nucleus:

$$v \cdot t_{lab} \leq R_A \approx r_0 A^{\frac{1}{3}}$$

"Coherence length"

Coherence length $\equiv$ formation time for elastic or quasielastic interactions.

Given a two body interaction between with four-momentum transfer

$$q = p_{1i} - p_{1f}$$

the energy transfer seen in a frame where the particle 2 is at rest is given by

$$\Delta E_2 \; = \; \nu_2 = \frac{q \cdot p_{2i}}{m_2}$$

From the uncertainty principle this ΔE corresponds to a indetermination in proper time given by $\Delta\tau \cdot \Delta E_2 = \hbar$, that boosted to the lab frames gives a coherence length

$$\Delta x_{lab} \; = \; \frac{p_{2lab}}{m_2} \cdot \Delta\tau = \frac{p_{2lab}}{m_2}\frac{\hbar}{\nu_2}$$

And analogue for particle 1

Can be applied also to $\nu - h$ interactions

Preequilibrium

For E $>$ π production threshold $\rightarrow$ only (G)INC models

At lower energies$\rightarrow$ a variety of preequilibrium models

Two leading approaches

the quantum-mechanical multistep model	the exciton model
Very good theoretical background	statistical assumptions
complex, difficulties for multiple emission	simple and fast

Exciton model: chain of steps, each (n_{th}) step corresponding to N_n

"excitons" == either a particle above or a hole below the Fermi surface

Statistical assumption: any partition of the excitation energy E among N, $N = N_h + N_p$, excitons has the same probability to occur

Step: nucleon-nucleon collision with $N_{n+1} = N_n + 2$ ("never come back" approximation)

Chain end = equilibrium = N_n sufficiently high or excitation energy below threshold

N_1 depends on the reaction type and on the cascade history

Preequilibrium : GDH

Preequilibrium emission probability:

$$P_{x,n}(\epsilon)d\epsilon = \sum n_{p_x} \frac{\rho_n(U,\epsilon) g d\epsilon}{\rho_n(E)} \frac{r_c(\epsilon)}{r_c(\epsilon) + r_+(\epsilon)}$$

where the density (MeV^{-1}) of exciton states is given by:

$$\rho_n(E) = \frac{g(gE)^{n-1}}{n!(n-1)!}$$

the emission rate in the continuum:

$$r_c = \sigma_{inv} \frac{\epsilon}{g_x} \frac{(2s+1)\, 8\pi m}{h^3}$$

and the reinteraction rate:

$$r_+(\epsilon) = f_{Pauli}(\epsilon, E_F) \left[\rho_p \sigma_{xp} + \rho_n \sigma_{xn}\right] \left[\frac{2(\epsilon + V)}{m}\right]^{1/2}$$

$$(or\ from\ optical\ potential)$$

GDH: ρ,E_F are "local" averages on the trajectory and constrained exciton state densities are used for the lowest lying exciton configurations.

Preequilibrium/(G)INC transition

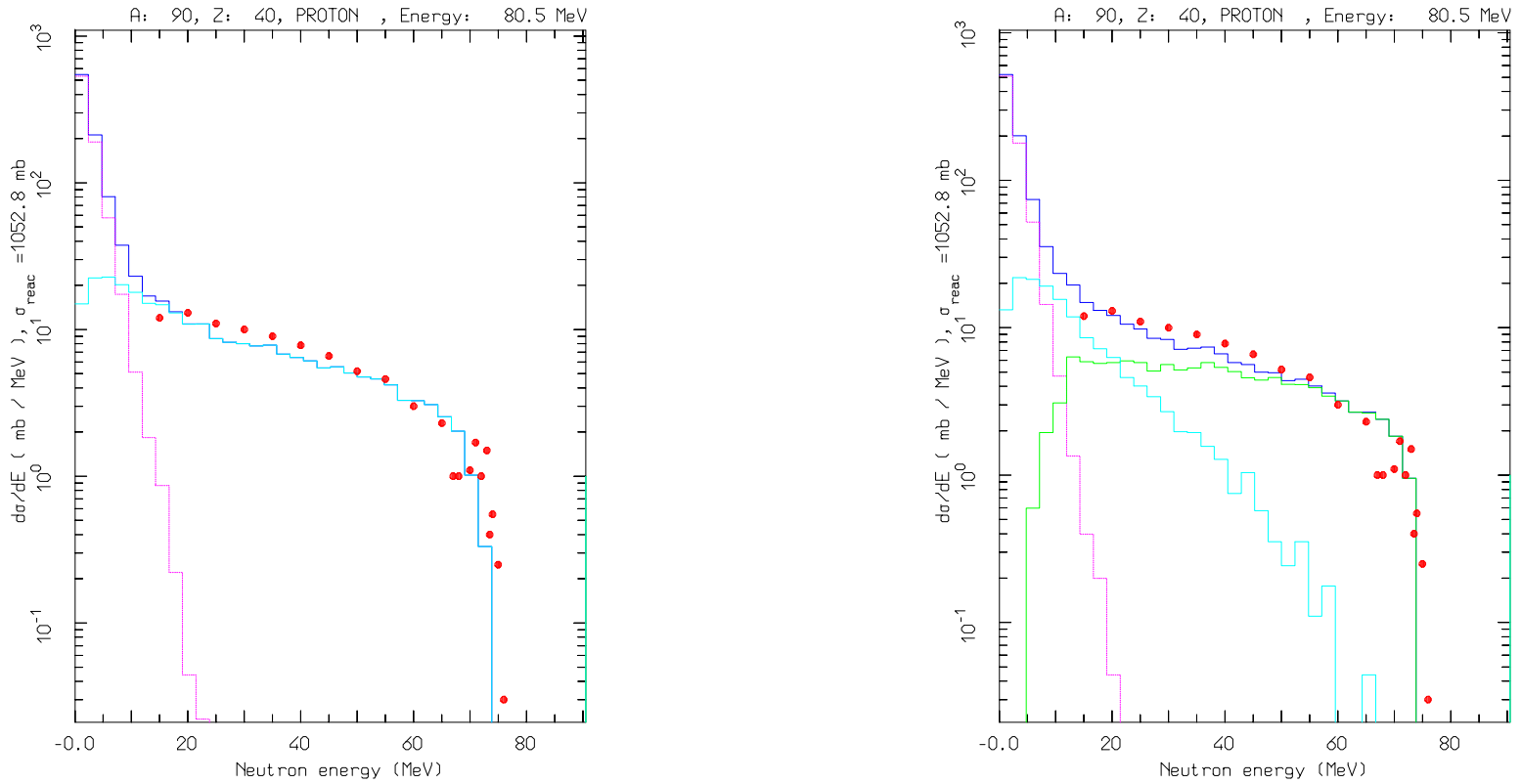

Example of angle integrated ^{90}Zr(p,xn) at 80.5 MeV calculations with the full algorithm (right), and without the INC stage (left). The various lines show the total, INC, preeq. and evaporation contributions, the exp. data have been taken from M.Trabandt et al. **PRC39** (1989) 452

Nonelastic interactions at intermediate energies: examples

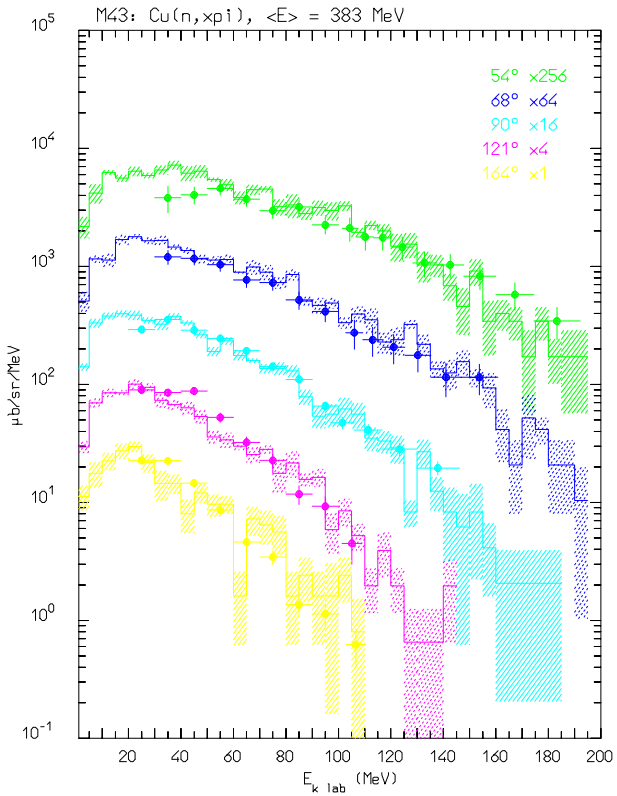

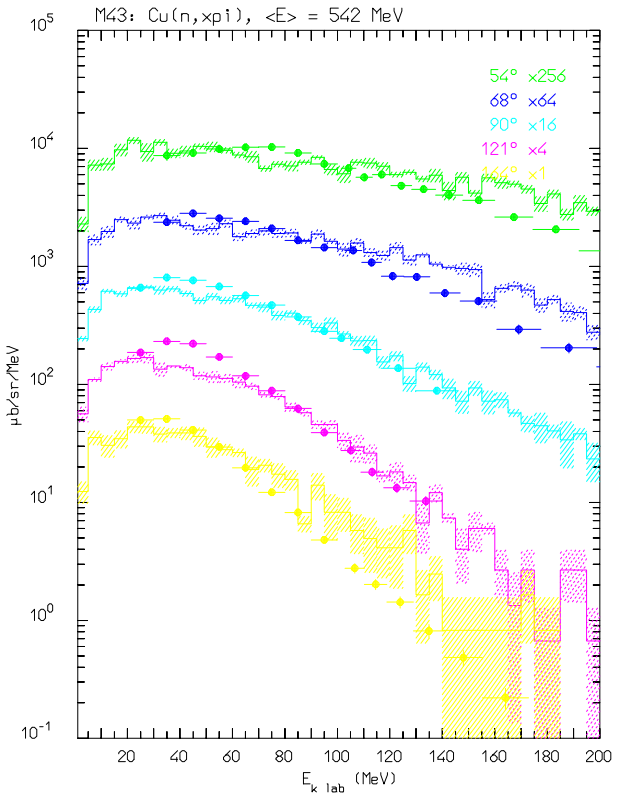

Double differential distributions of charged pions produced by neutrons of $< E_n >$=383 (left) and 542 MeV (right). Exp. data have been taken from Buchle et al. **NPA515**, (1990) 541

Nonelastic interactions at intermediate energies: examples II

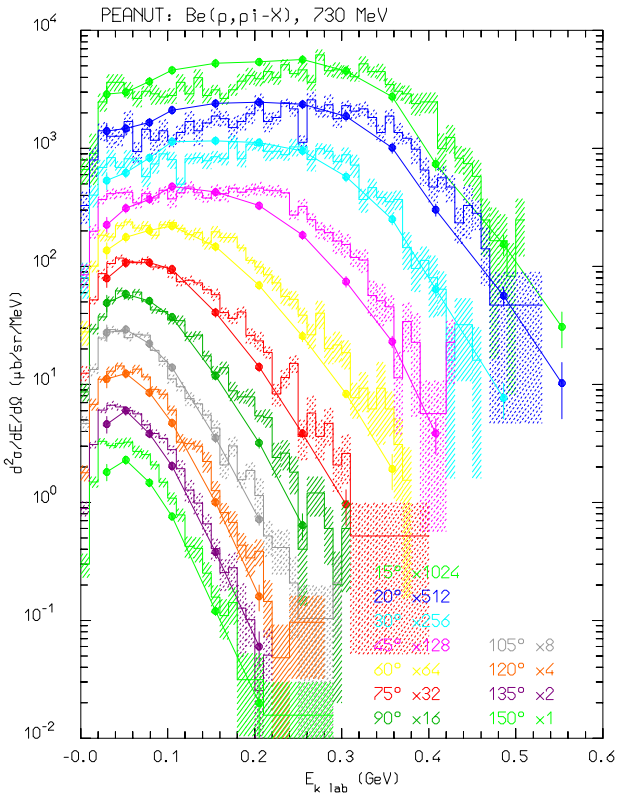

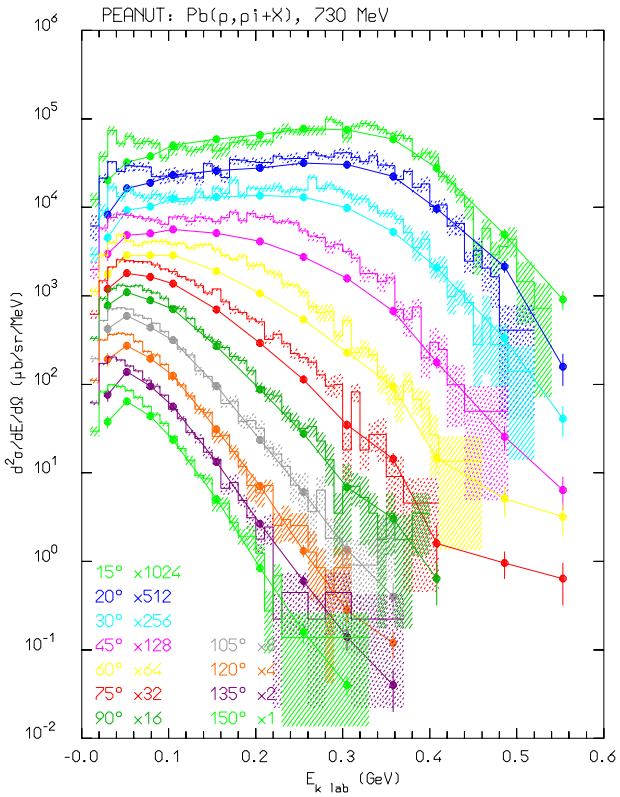

Double differential distributions of pions produced by 730 MeV protons. π^-'s from Be (left) and π^+ frpm Pb (right). Exp. data (symbols) have been taken from D.R.F. Cochran et al., **PRD6**, (1972)

Nonelastic interactions at intermediate energies: examples III

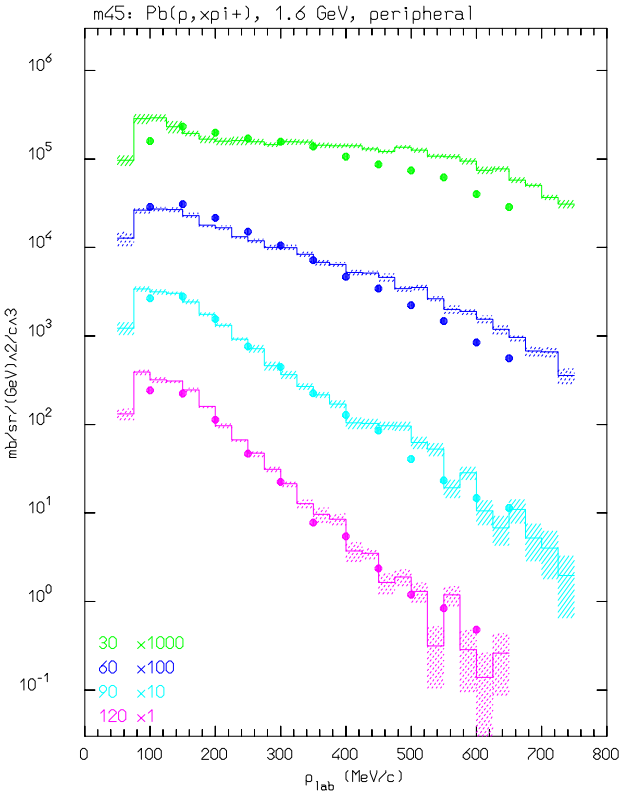

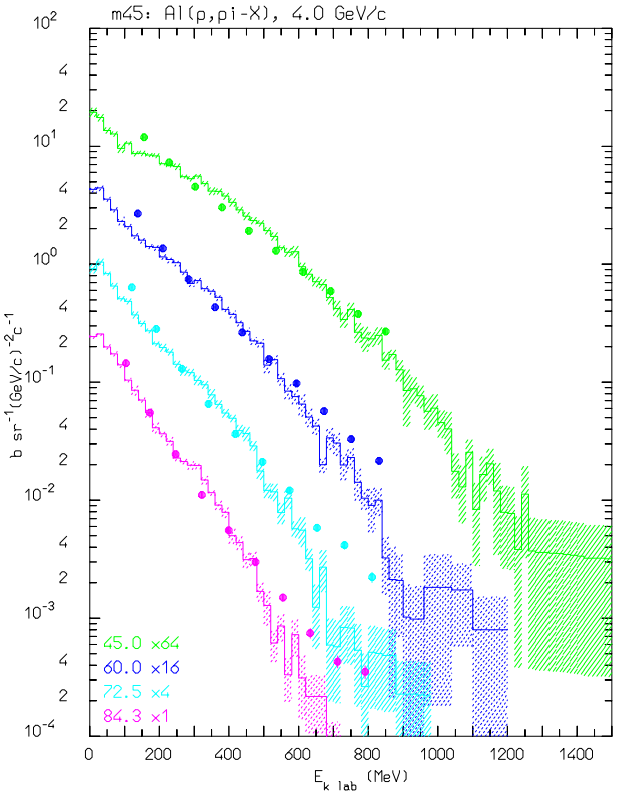

Double differential distributions of π^+'s produced by 1.6 GeV protons on Pb (left, exp. data from M.C.Lemaire et. al., CEA-N-2670) and π^- produced by 4 GeV/c protons on Al (right, exp data from H. En'yo et al, PL 159B, 1 (1985)).

Pion interactions in nuclei

The description of pion interactions on nuclei in the sub-GeV energy range must take into account:

- The resonant nature of the $\pi - N$ interaction, mostly dominated by the $\Delta(1232)$.
- The effect of the nuclear medium on the $\pi - N$ interaction
- The possibility of absorption (both s-wave and p-wave) on two or more nucleons
- The resonant nature of the pion-nucleus potential, which is rapidly varying with the pion energy

The importance of in flight pion absorption

Both positive and negative pions can be absorbed in flight through multi-nucleon processes in nuclei. These processes are particularly important at subGeV energies

$\Downarrow$

- Competition with charge exchange strongly reduces the EM component
- Weakly ionizing relativistic particles are converted into heavily ionizing protons and energetic neutrons $\rightarrow$ signal losses

This process impacts the e/h ratio at all energies as well as resolutions at low-medium energies. It is critical for Cerenkov calorimeters

Microscopic pion absorption cross sections

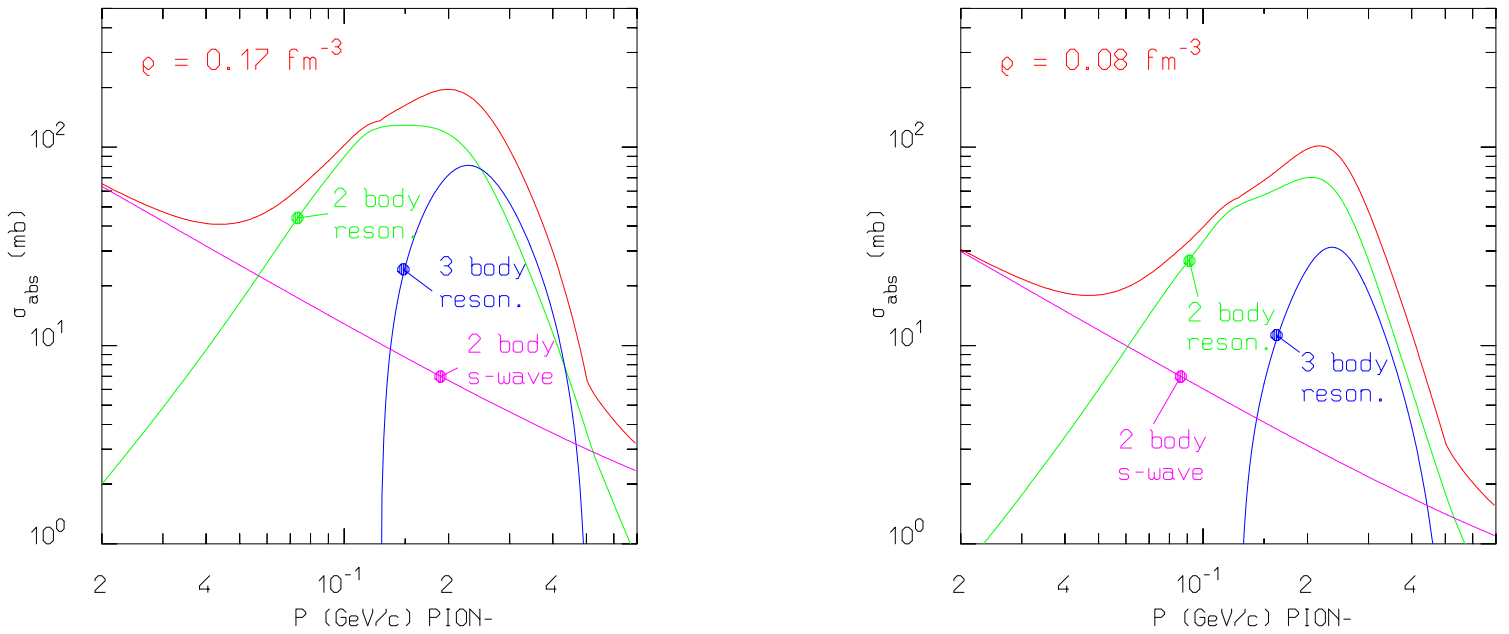

Charged pion absorption cross section for infinite symmetric nuclear matter at two different density values ($\lambda_{abs}^{-1} = \sigma_{abs} \cdot \frac{1}{2}\rho = \sigma_{abs} \cdot \rho_{pro} = \sigma_{abs} \cdot \rho_{neu}$)

Pion absorption cross sections: examples

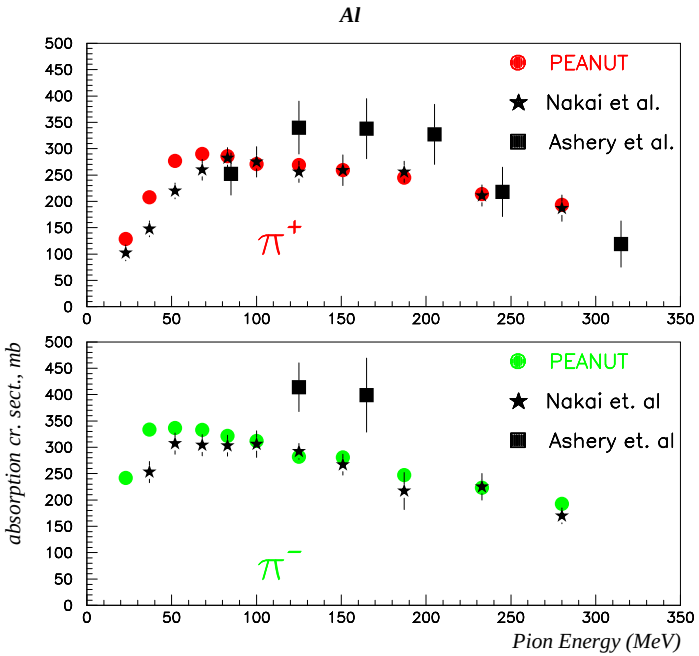

Computed and exp. pion absorption cross section on Aluminum as a function of energy

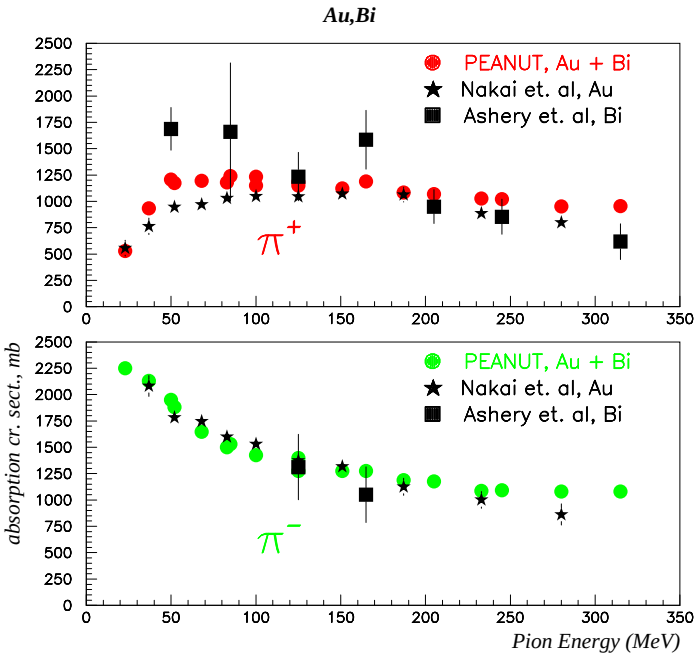

Computed and exp. pion absorption cross section on Gold or Bismuth as a function of energy

(Exp. data: D. Ashery et al., **PRC23**, (1981) 2173 and K. Nakai et. al., **PRL44**, (1979) 1446)

Pion interactions: examples

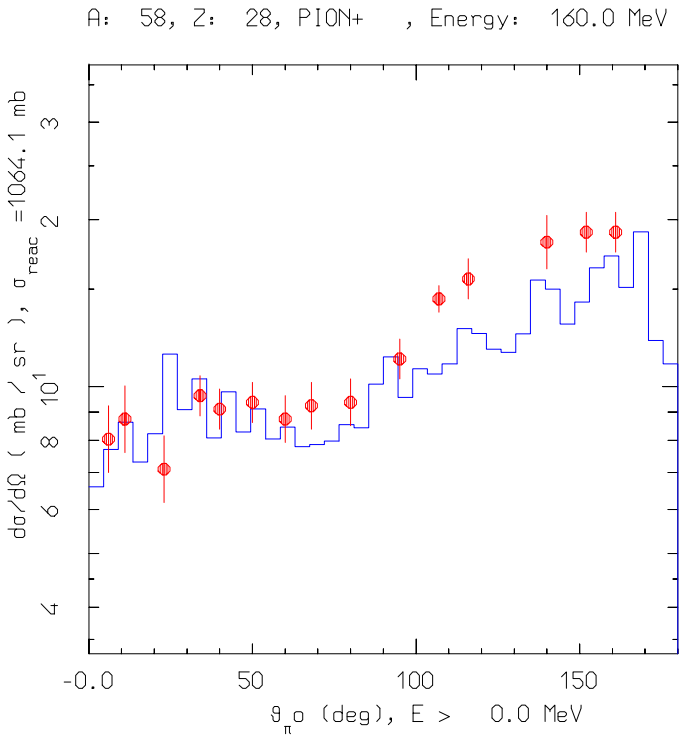

Computed and exp. pion charge exchange angular distribution for ^{58}Ni(π^+, π^0) at 160 MeV

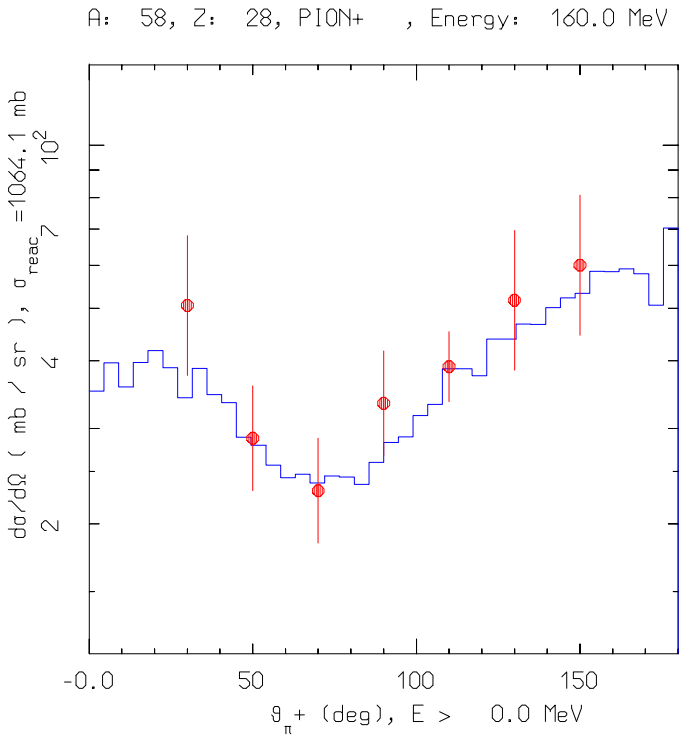

Computed and exp. pion inelastic angular distribution for ^{58}Ni$(\pi^+, \pi^{+\prime})$ at 160 MeV

(Exp. data: W.J. Burger et al., **PRC41**, (1990) 2215, R.D. McKeown et al.,**PRC24**, (1981) 211

Evaporation, fission and nuclear break-up

The evaporation probability for a particle of type j , mass m_j, spin $S_j \cdot \hbar$ and kinetic energy E and the total fission probability are given by

$$P_j = \frac{(2S_j+1)m_j}{\pi^2\hbar^3}\int_{V_j}^{U_i-Q_j-\Delta_f}\sigma_{\text{inv}}\frac{\rho_f(U_f)}{\rho_i(U_i)}EdE$$

$$P_F = \frac{1}{2\pi\hbar}\frac{1}{\rho_i(U_i)}\int_0^{(U-B_F)}\rho_F(U-B_F-E)dE$$

- ρ's: nuclear level densities ($\rho_f(U_f)$ for the final nucleus, $\rho_i(U_i)$ for the initial one, $\rho_F(U_F)$ for the fissioning nucleus at the saddle point),
- $U_i \equiv U$: excitation energy of the evaporating nucleus,
- $U_f = U - E - Q_j$: that of the final one,
- $U_F = U - B_F$: excitation energy of the fissioning nucleus at the saddle point (B_F is the fission barrier)
- Q_j: reaction Q for emitting a particle of type j,
- V_j: (possible) Coulomb barrier for emitting a particle of type j,
- σ_{inv}: cross section for the inverse process.

Evaporation, fission and nuclear break-up cont.d

The level density can be assumed to be:

$$\rho(U)dU = \frac{e^{2\sqrt{a(U-\Delta)}}}{12\sqrt{\pi}a^{\frac{1}{4}}(U-\Delta)^{\frac{5}{4}}}dU$$

$$P_j(E)dE \approx K\ Ee^{-\frac{E}{T}}dE$$

- a: level density parameter ($\approx A/8$ MeV^{-1})
- Δ: pairing energy
- T: nuclear temperature (MeV), ($T \approx \sqrt{(U-\Delta)/a}$)

- *Neutrons emission is favoured for medium-heavy nuclei*
- *For the same excitation, the neutron multiplicity is larger for heavier nuclei*
- *The excitation is higher for heavier nuclei due to the larger cascading chances*

h-A interactions: the electromagnetic component

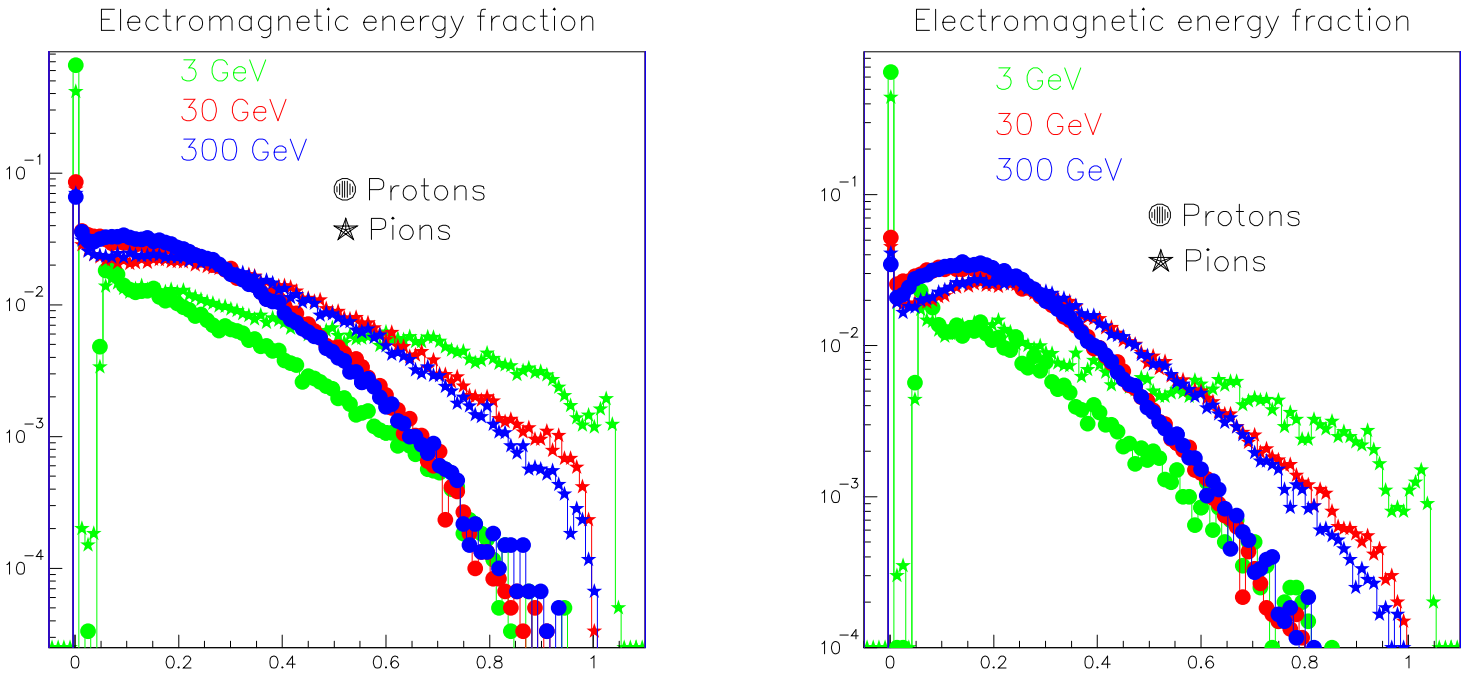

Distribution of the energy fraction carried by π^0's and γ's for interactions in aluminium (left) and lead (right)

h-A interactions: the scaling of the electromagnetic component

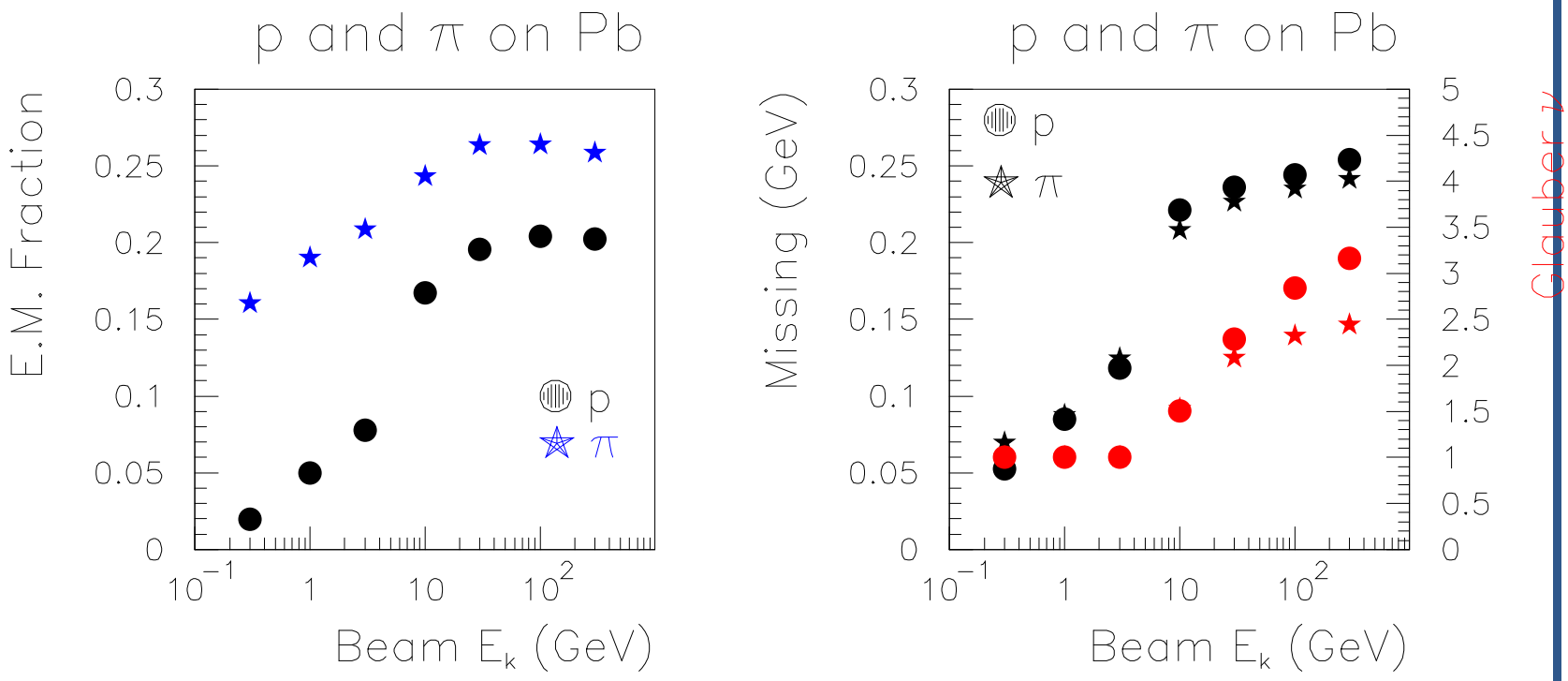

Average energy fraction carried by π^0's and γ's (left) and binding energy losses (right) for interactions in lead. The number of primary collisions are also reported in the last plot

h-A at high energies: the invariance of the target fragmentation region

The Glauber cascade and the formation zone act together in reaching a regime where the "slow" part of the interaction is almost independent of the particle energy

This regime can be easily verified looking at charged particle average multiplicities and multiplicity distributions as a function of energy

- "Fast" tracks, coming from the projectile primary interactions, show the typical $\approx$ logarithmic increase observed for hN interactions
- "Gray" tracks, mostly due to intranuclear cascade reinteractions tend to saturate just above 10 GeV
- "Black" tracks, mostly due to evaporation charged particles saturate as well

Nonelastic hA interactions at high energies: examples

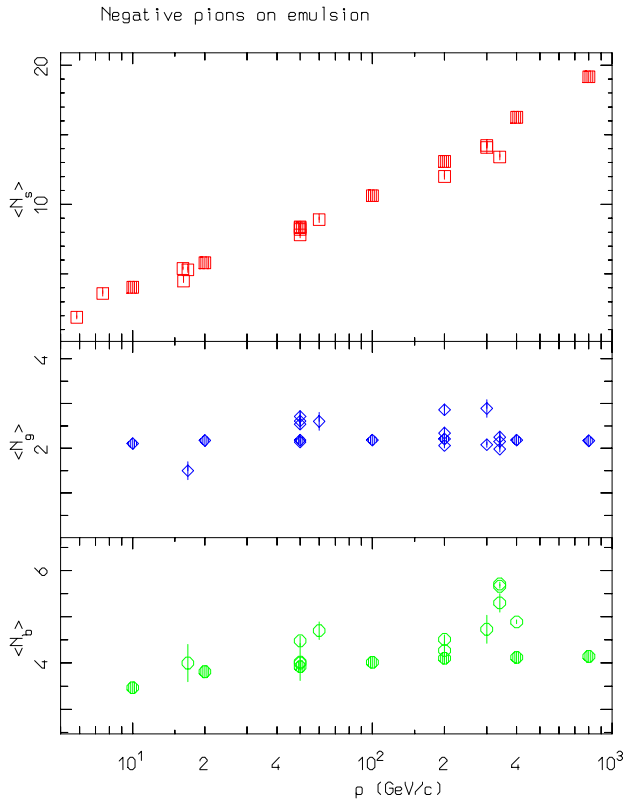

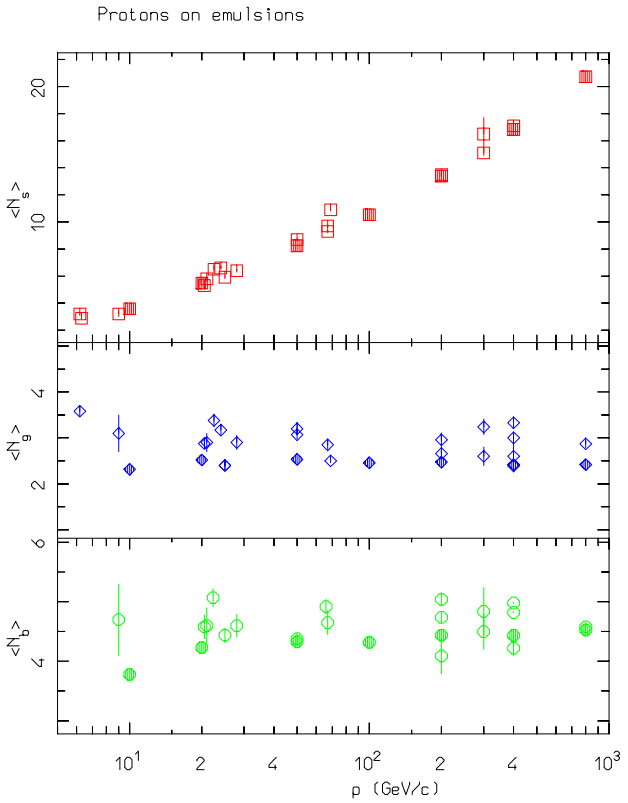

Shower, grey, and black tracks multiplicities for π^- (left) and protons (right) incident on emulsion, as a function of the projectile momentum. Open symbols are experimental data from various sources, full symbols are FLUKA results.

Nonelastic hA interactions at high energies: examples II

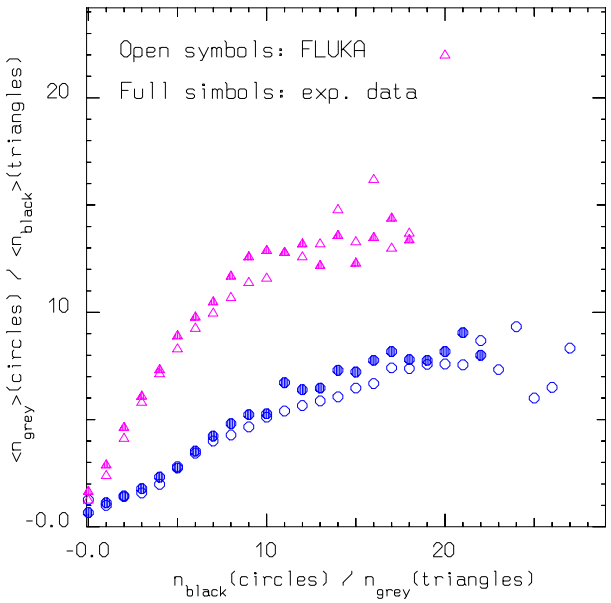

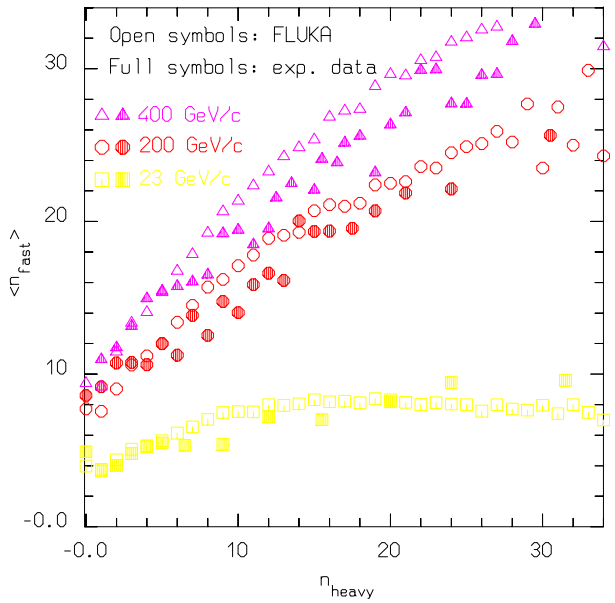

Correlation between the number of heavy prongs and fast particle multiplicity for protons on emulsion at various momenta, and mutual correlations ($< n_g >$ vs n_b and $< n_b >$ vs n_g) between black and grey charged tracks for 400 GeV/c p on emulsion. Open symbols are experimental data from various sources, full symbols are FLUKA results.

Nucleon emission: thin target examples I

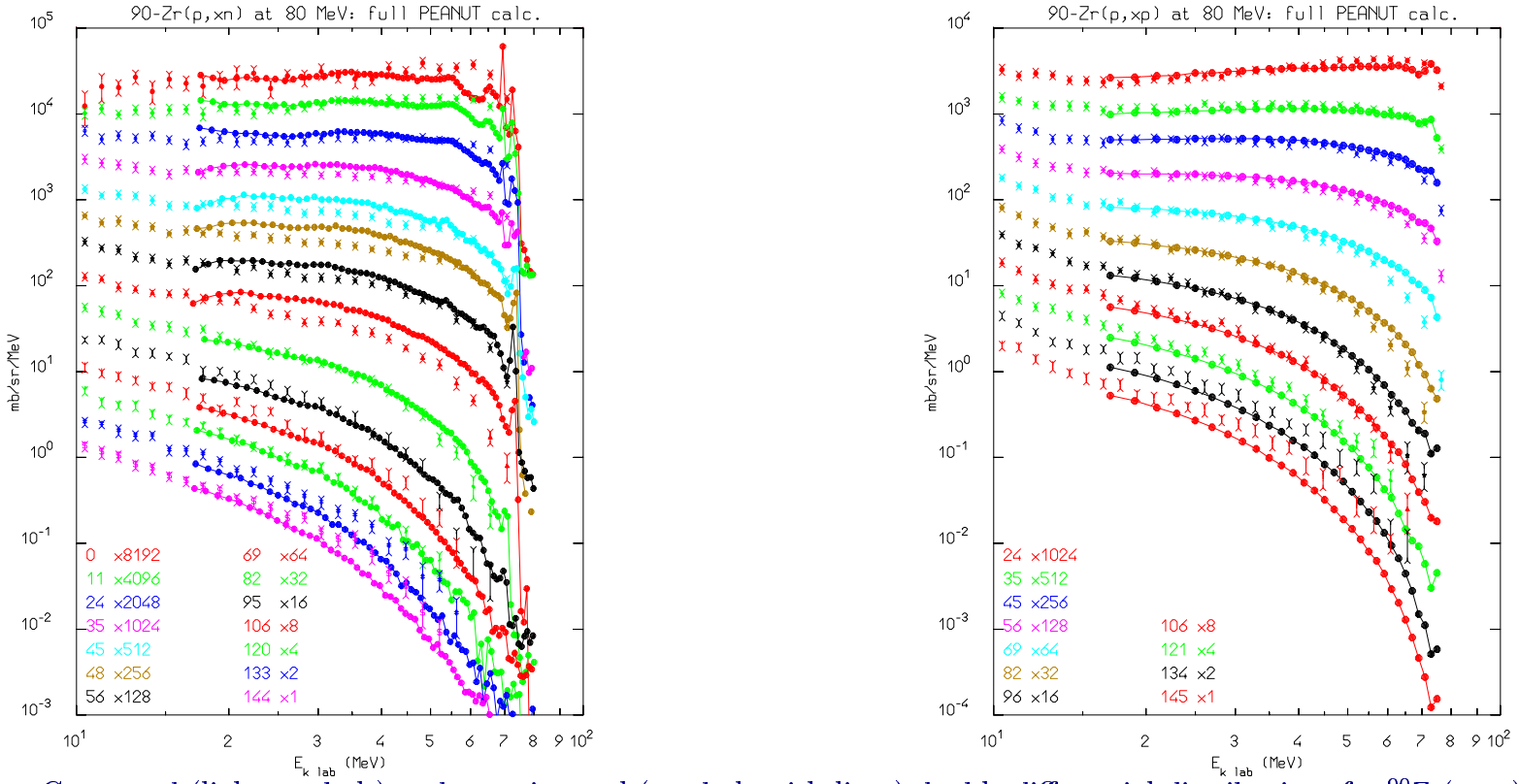

Computed (light symbols) and experimental (symbols with lines) double differential distributions for ^{90}Zr(p,xn) (left) and ^{90}Zr(p,xp) at 80.5 MeV. The exp. data have been taken from M.Trabandt et al. **PRC39** (1989) 452 and A.A. Cowley et al., **PRC43**, (1991) 678

Nucleon emission: thin target examples I

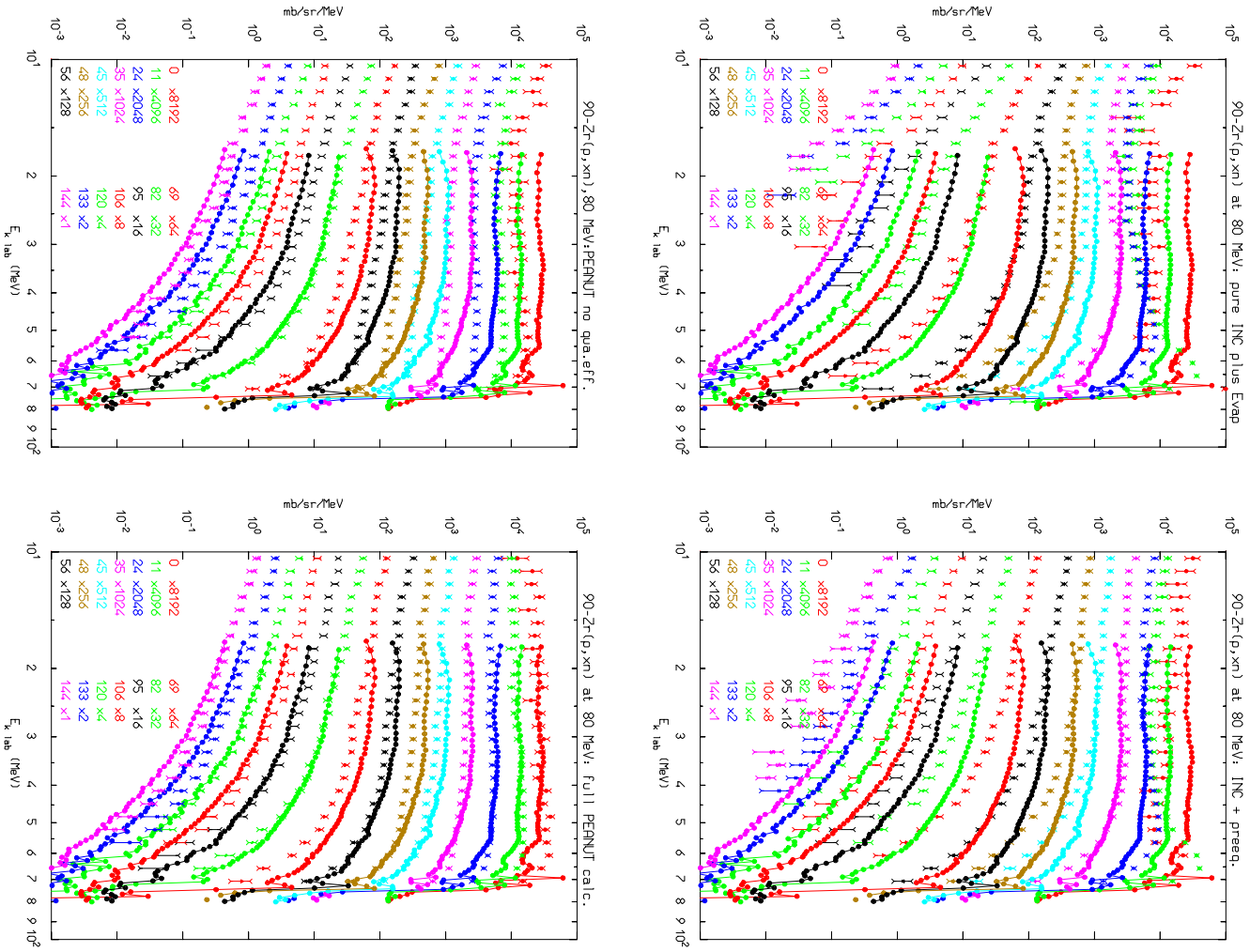

Nucleon emission: thin target examples I

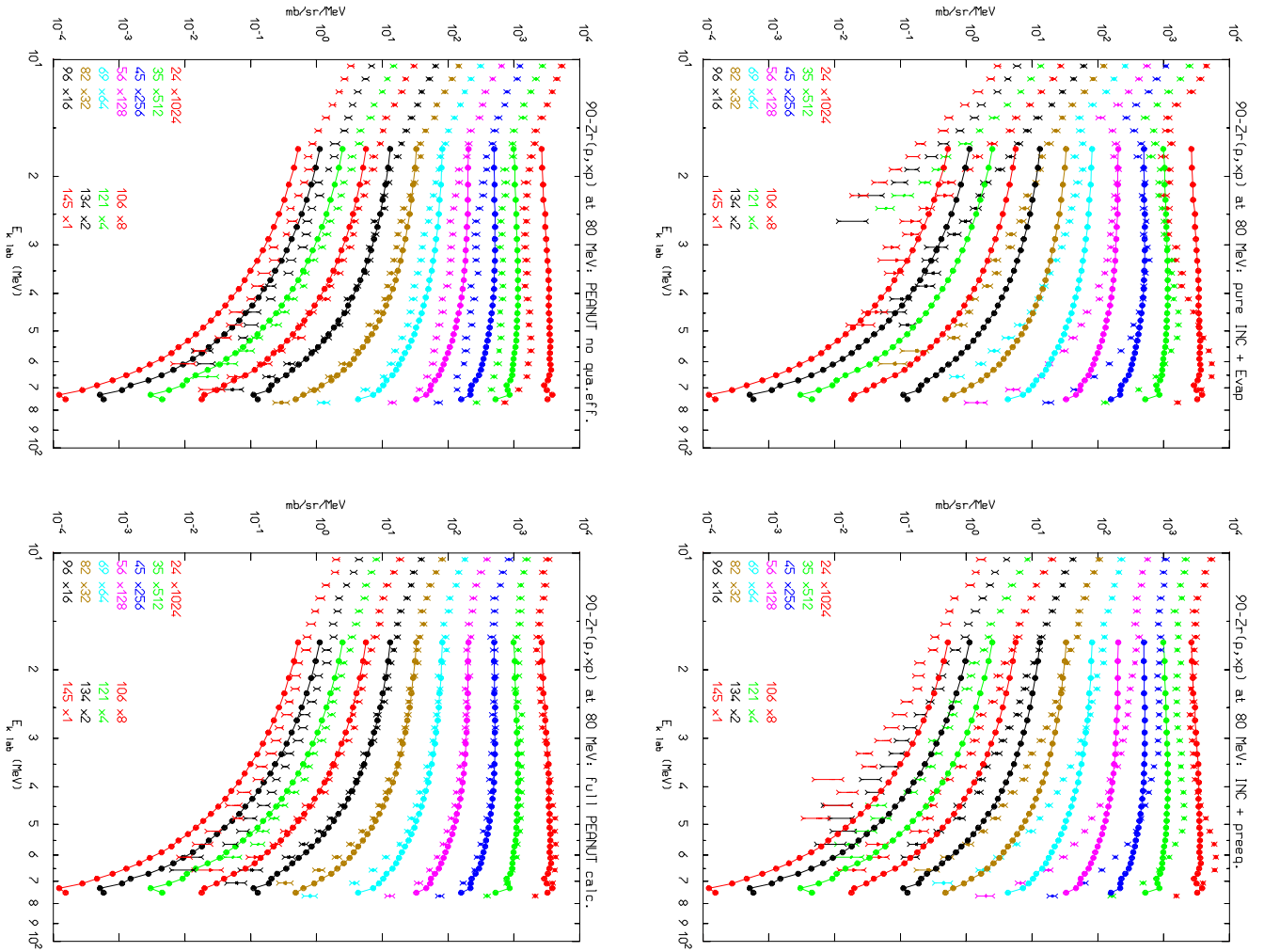

Nucleon emission: thin target examples II

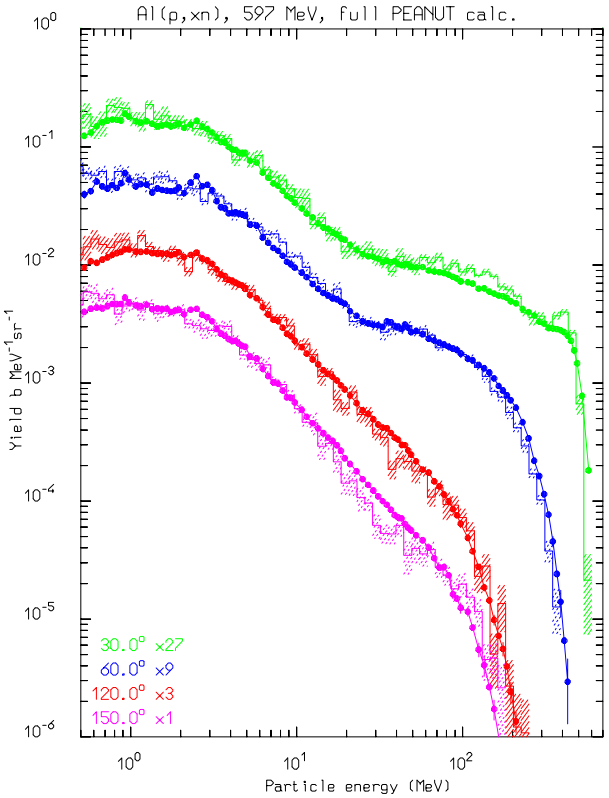

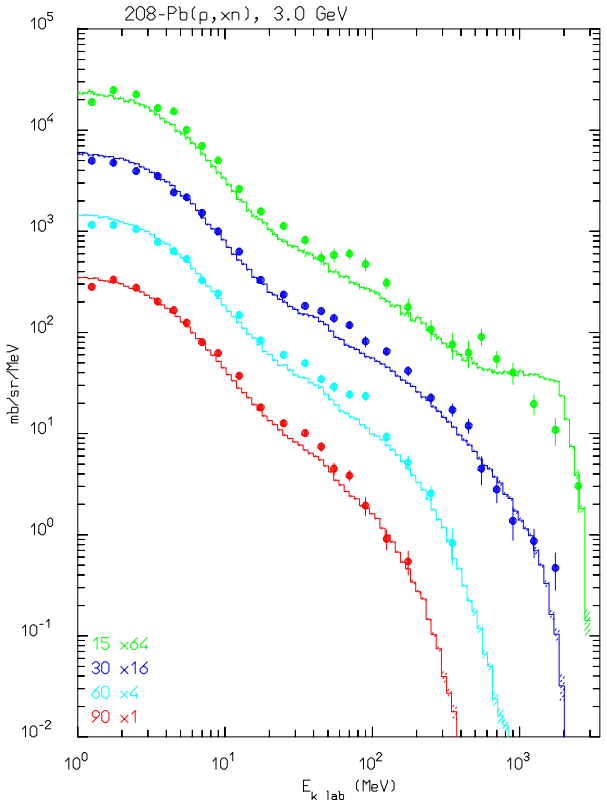

Computed (histograms) and experimental (symbols) double differential neutron distributions for Al(p,xn) (left) at 597 MeV and Pb(p,xn) at 3 GeV. The exp. data have been taken from W.B. Amian et al., Nucl. Sci. Eng. **115**, (1993) 1, and K. Ishibashi et al, Nucl. Sci. Technol. **32** (1995) 827.

Residual nuclei: a test of evaporation and binding energy losses predictions

The production of residuals is a powerful check about the correctness of intranuclear cascading and the slow stages of hadronic interactions

The predictions about production of specific isotopes have additional problems wrt the calculation of emission spectra

- Small changes in the final evaporation steps can lead to fairly different residuals with little or no impact on the emitted spectra
- Nuclear structure effects play a major role which cannot be easily accounted for
- The lack of spin-parity dependent calculations in most MonteCarlo models limits their accuracy
- Fragmentation processes are known to populate the mass range A<20-30 for medium/heavy target nuclei. These processes are difficult to model in MonteCarlo codes.
- Isomer production: an open question
- The range of interesting cross section values typically spans *four* order of magnitudes

Fortunately for most purposes the residual mass distribution is a proper index of reliability. *This is no longer the case when the interest is in specific isotope production!*

Residual nuclei: the mass distribution at high energies

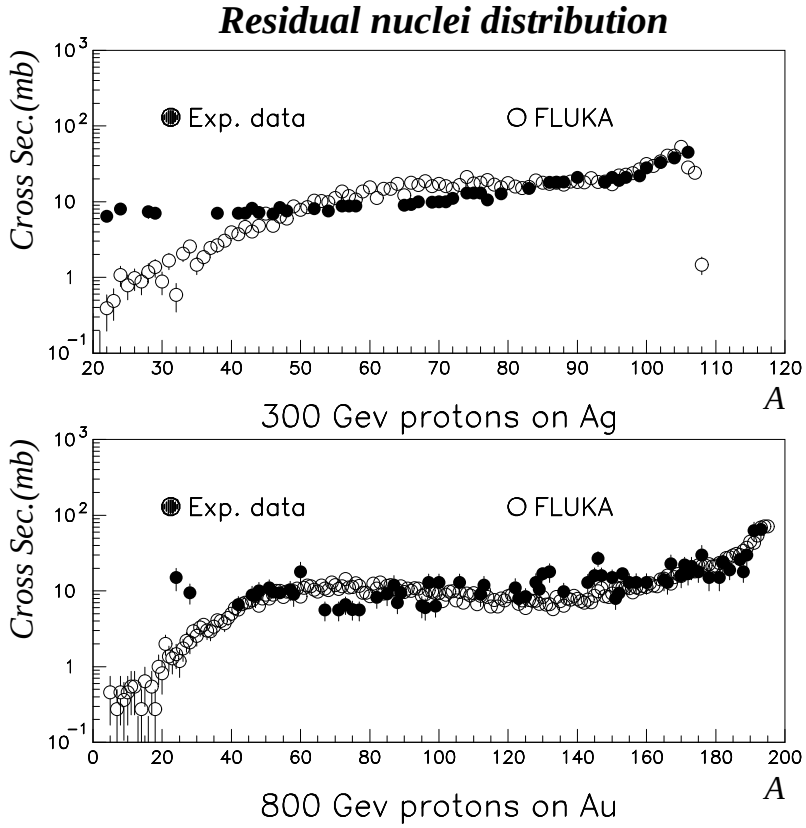

Experimental and computed residual nuclei mass distribution following for Ag(p,x)X at 300 GeV (top) and Au(p,x)X at 800 GeV (bottom).

Residual nuclei predictions: a look at the isotope table

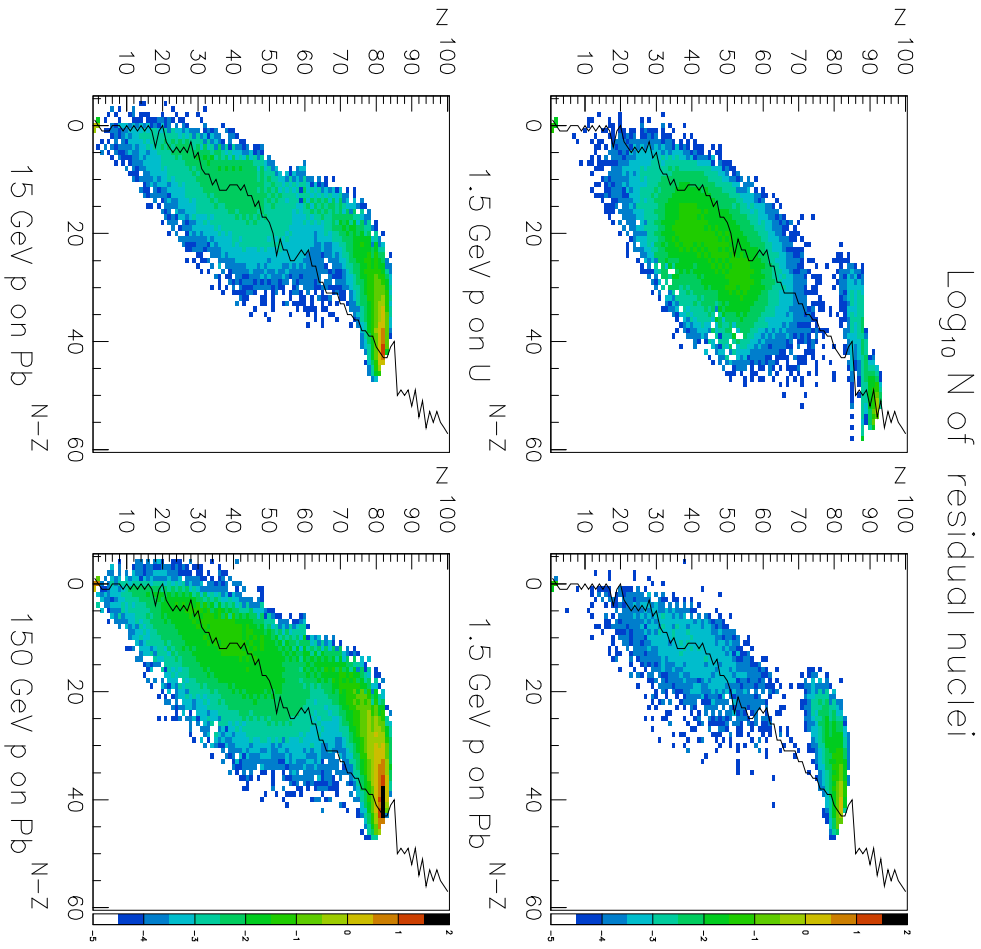

Energy conservation and its relevance for sound calorimetric calculations

A fraction of the incoming energy in hadronic interactions is spent via mass production. Binding energy losses and their fluctuations are indeed an important ingredient, particularly at low projectile energies, both in determining the e/h ratio and the intrinsic resolution for hadronic showers.

A precise calculation of such losses can be easily performed using self-consistent interaction models fulfilling the basic conservations laws, energy, momentum and additive quantum numbers:

$$E_{k\ proj} + m_{proj} + {}^{A}_{Z}M \;=\; \sum_i \left[E_{k\ i} + m_i\right] + \sum_j \left[E_{k\ j} + {}^{A_j}_{Z_j} M_j\right]$$

Assuming meson masses can be recovered and antibaryons will eventually annihilate:

$$E_{loss} \;=\; \sum_i \left[I_{bar\ i} \cdot m_i\right] + \sum_j \left[{}^{A_j}_{Z_j} M_j\right] - I_{bar\ proj} \cdot m_{proj} - {}^{A}_{Z}M$$

$$I_{bar\ diff} \;=\; A - \sum_j A_j = \sum_i I_{bar\ i} - I_{bar\ proj}$$

It turns out that (obviously):

$$E_{loss} \;\approx\; 8 \times I_{bar\ diff}\ \mathrm{MeV}$$

Energy conservation: examples

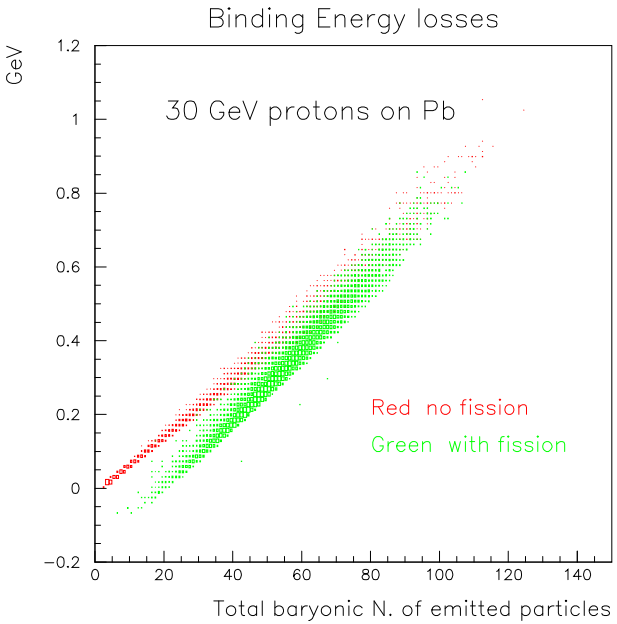

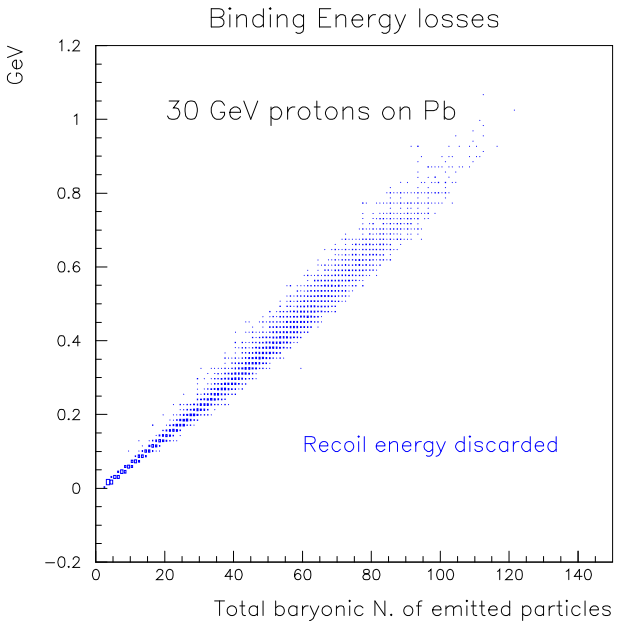

Binding energy losses for 30 GeV protons on lead (left). Binding energy losses plus heavy recoil energy for the same reaction (right)

"Low" energy neutrons

In bulk showers, the fraction of visible energy due to neutrons below 10-20 MeV is still very significant. Most of their kinetic is spent via elastic interactions.

Recoils are usually heavily quenched and a significant fraction of the energy is going into non ionizing recoils, except in the case of hydrogen.

Most of the low energy neutron contribution comes from capture γ rays. The capture probability is maximal in the thermal region: thermalization times can vary from μs to ms depending on the material composition

In principle if the capture γ ray contribution could be fully accounted for most of the binding energy losses would be recovered

Neutron production examples: thick targets

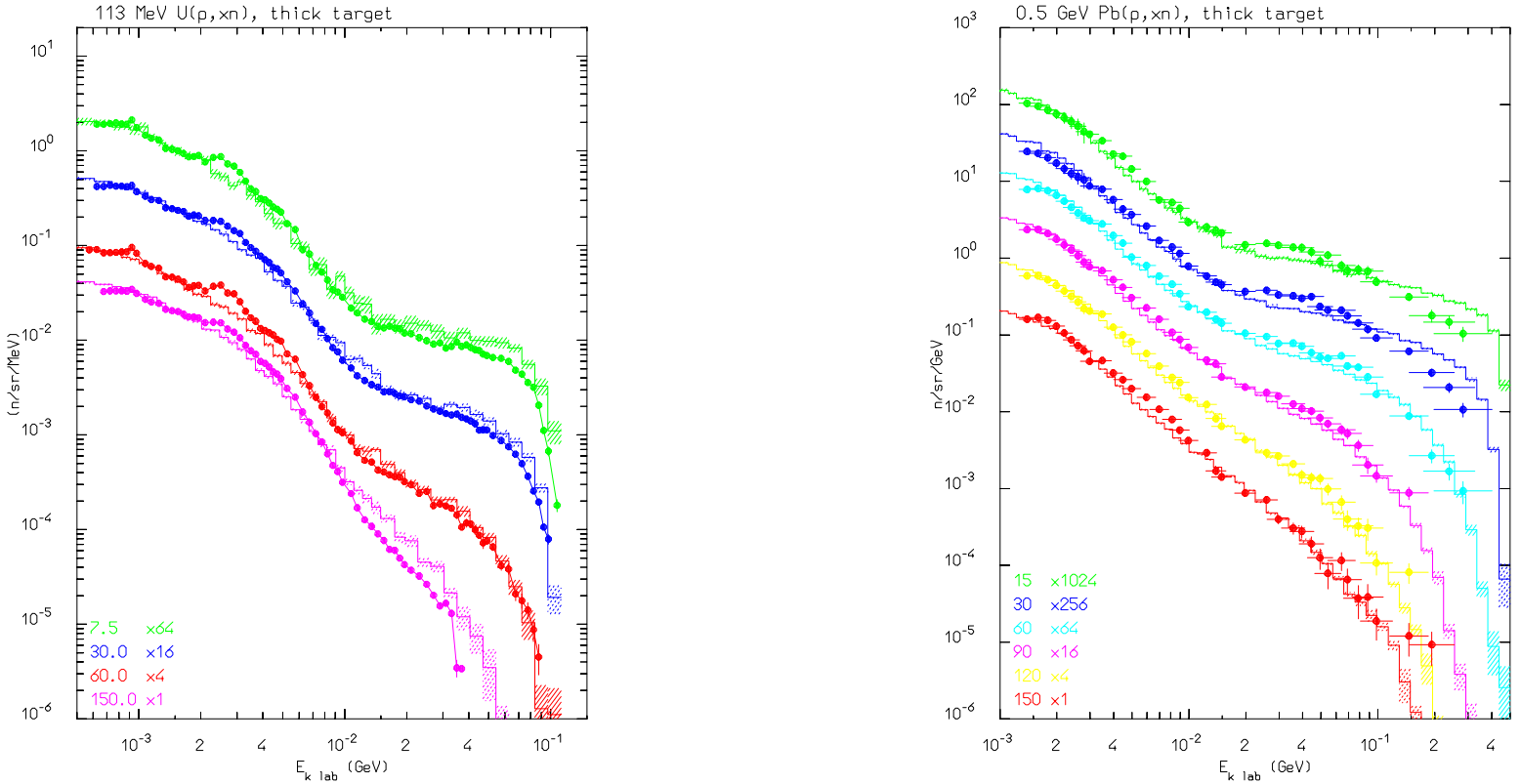

Simulated (dashed histogram) and experimental (symbols) neutron double differential distributions out of stopping length targets for 113 MeV protons on U (left, data from M.M. Meier et al., Nucl. Sci. Eng. **110**, (1992) 299) and 500 MeV protons on Pb and 256 MeV protons on uranium (right, S. Meigo et al., JAERI-Conf 95-008, (1995), 213)

Neutron production examples: TARC (PLB458 (1999) 167)

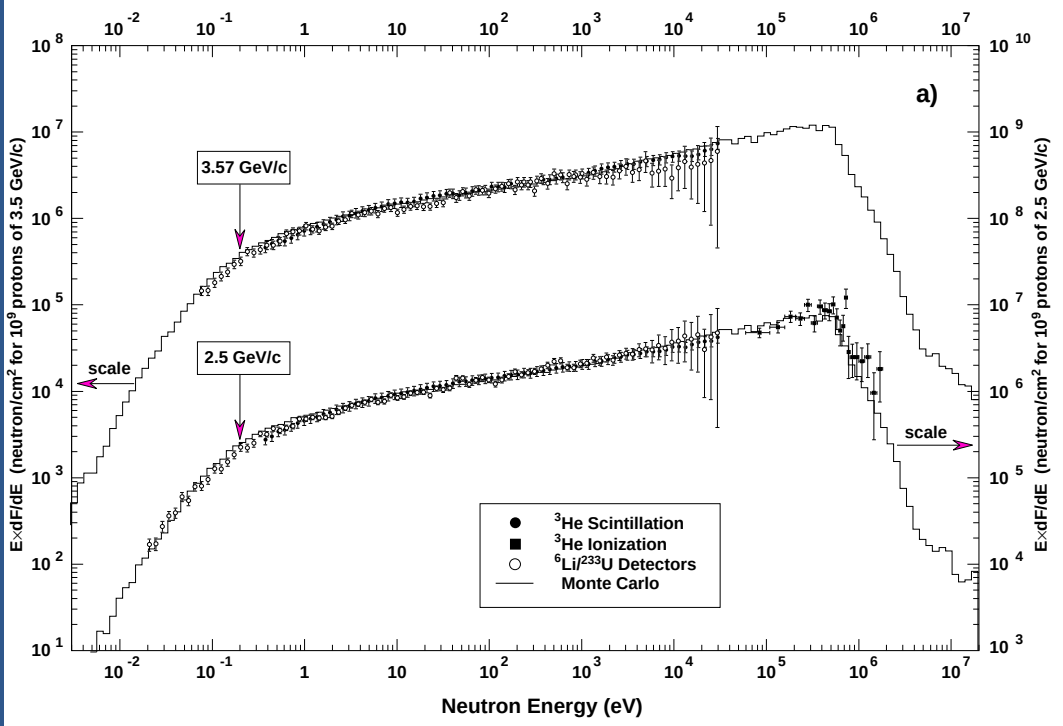

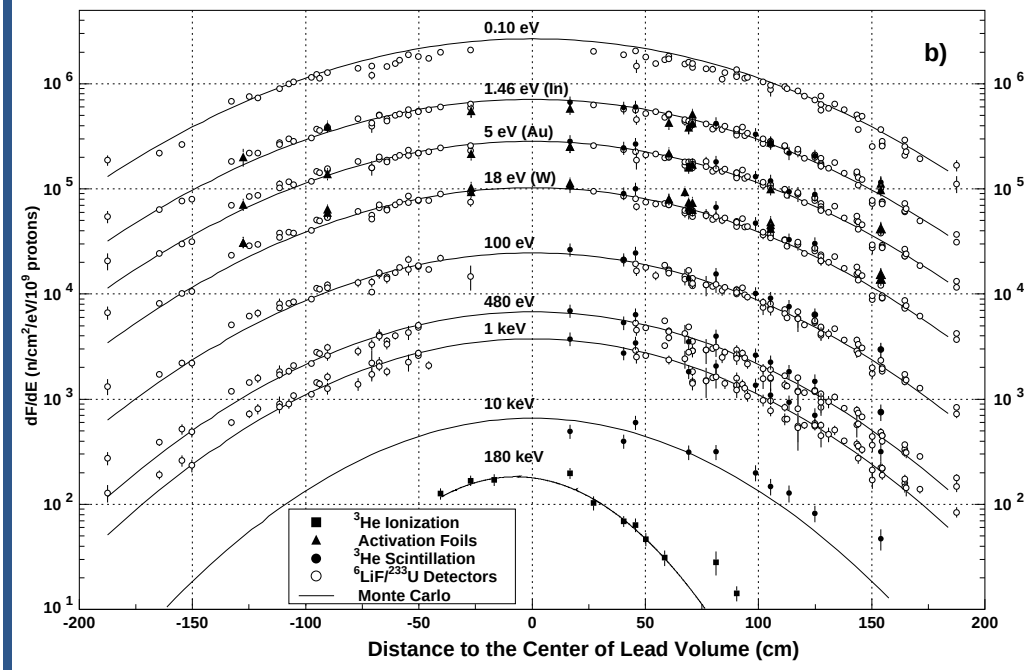

Infinite homogeneous calorimeters: some examples

Shower calculations at energies ranging from 1 to 300 GeV have been performed using infinite and homogeneous targets (Al, Fe, Pb and U)

The various contributions to a possible signal have been scored, together with the energy lost for binding and neutrinos.

In the following we will focus on the relative role of:

- The electromagnetic energy fraction
- The energy due to γ's produced by slow neutrons
- The energy spent in "heavy" (heavier than α's) recoils and fission fragments
- The energy lost due to binding

Infinite calorimeters: the electromagnetic component

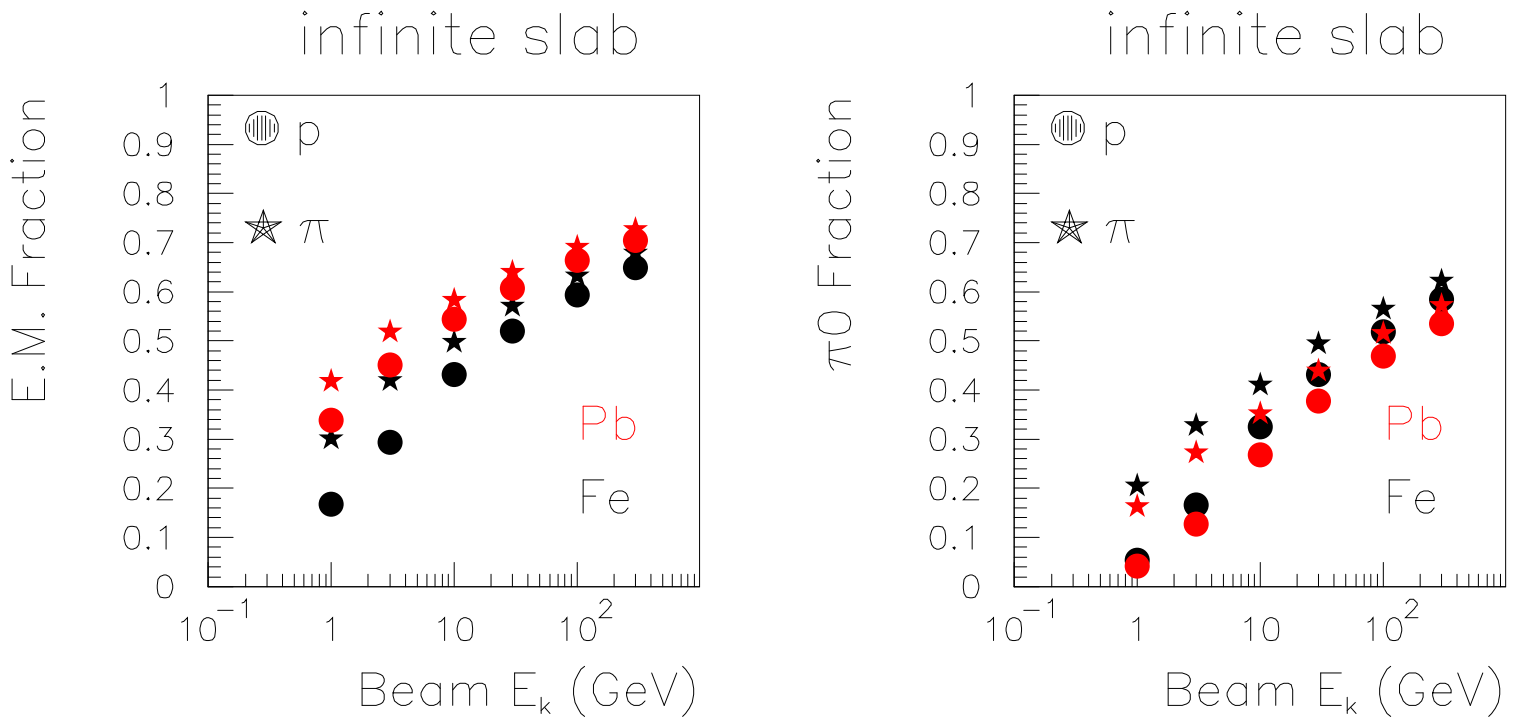

Energy fraction carried by π^0's and γ's for pion and proton showers (left). The same fraction without the slow neutron γ contribution (right)

Infinite calorimeters: binding losses

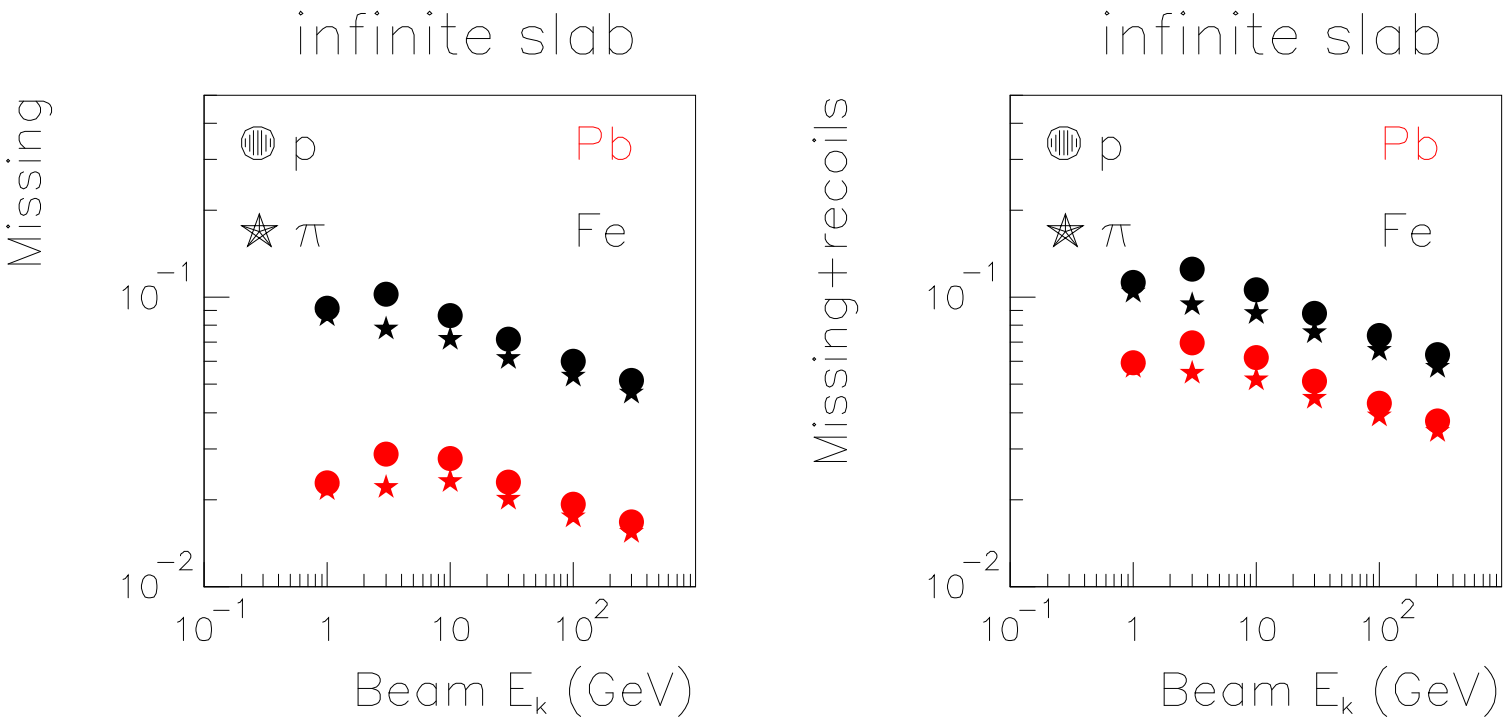

Average energy fraction "lost" due to binding for pion and proton showers (left). The same with in addition the energy due to heavy recoils and fission fragments (right)

Infinite calorimeters: the role of slow neutrons

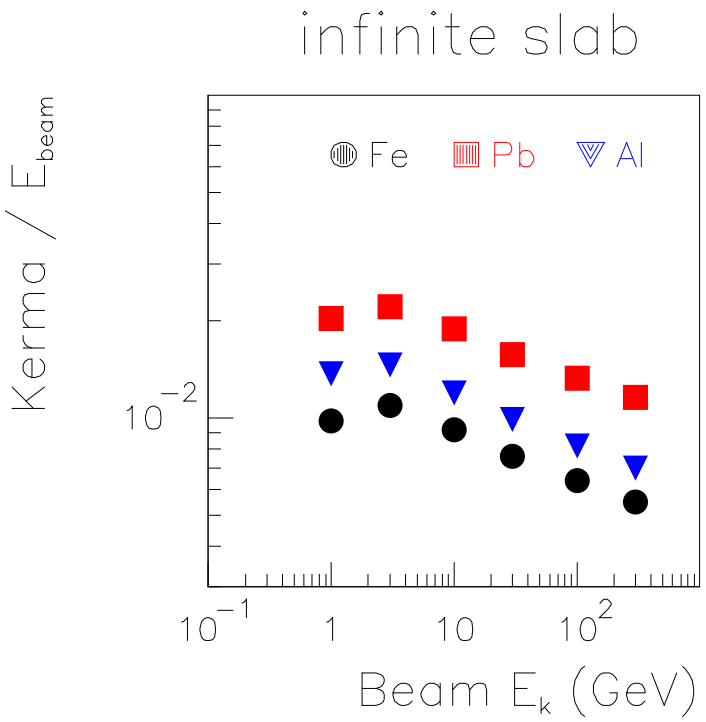

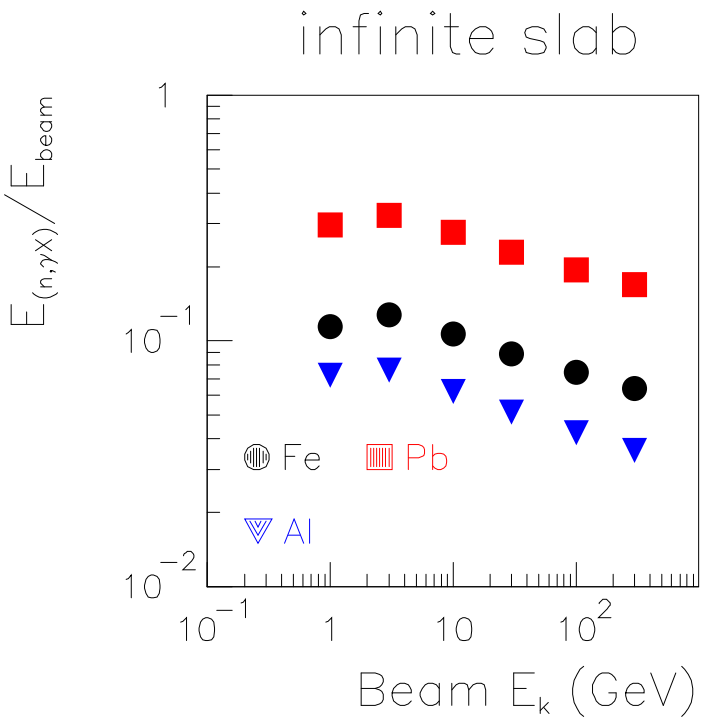

Average fractions of energy carried by "slow" neutrons, kinetic (left), and by γ's produced in (n,n') and capture reactions (right)

Infinite calorimeters: slow neutrons II

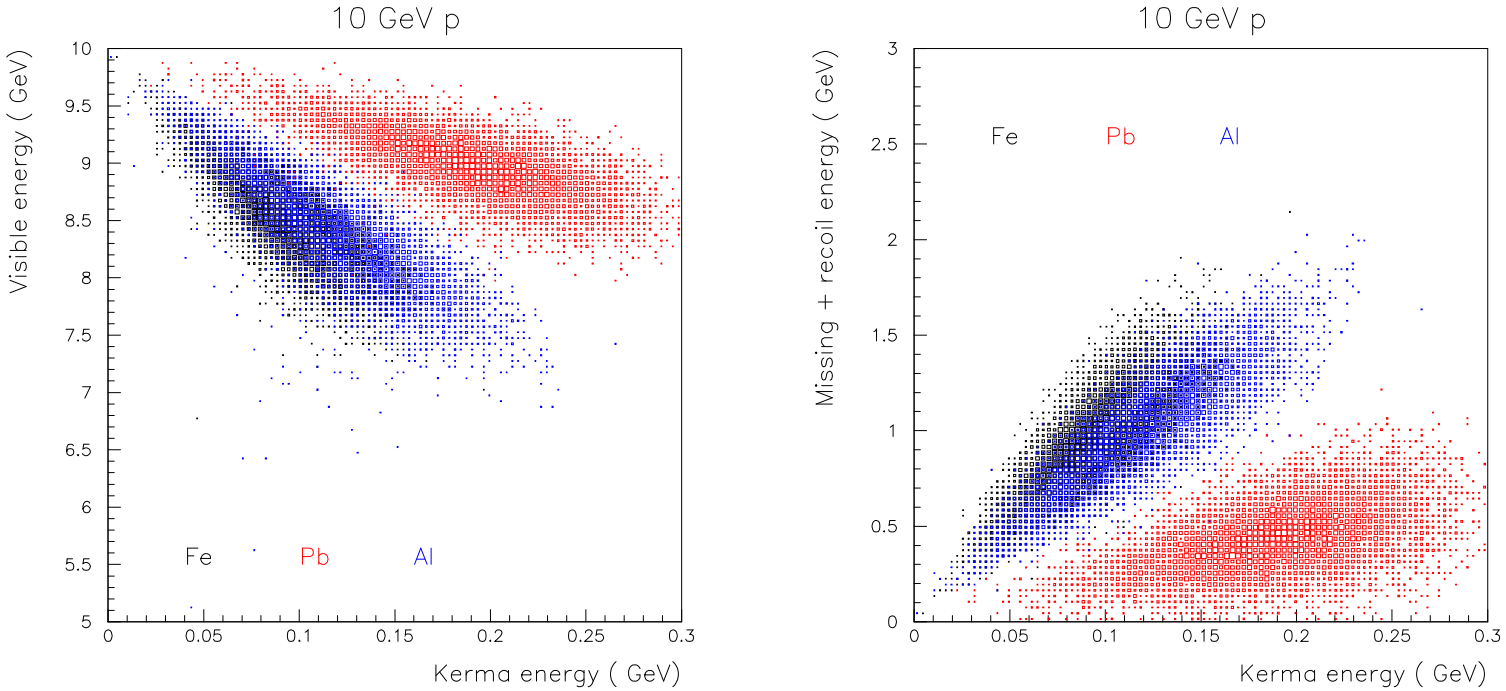

Correlation between slow neutron kinetic energy and (left) "visible" energy (everything but heavy recoils and fission fragments), (right) binding energy losses

Infinite calorimeters: slow neutrons III

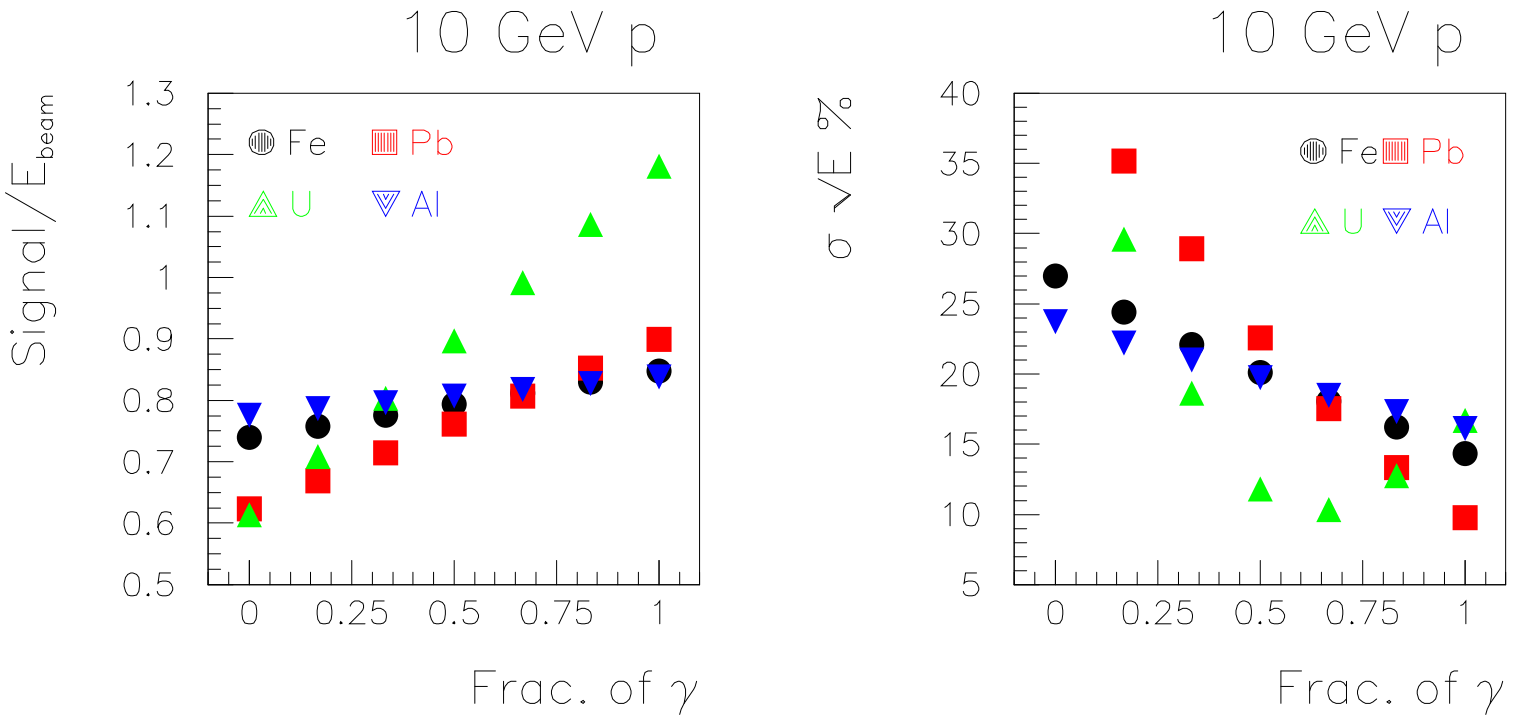

Average "visible" signal (left) (heavy recoil excluded, no quenching) and fractional resolution (right) as a function of the fraction of slow neutron γ's collected

Infinite calorimeters: slow neutrons IV

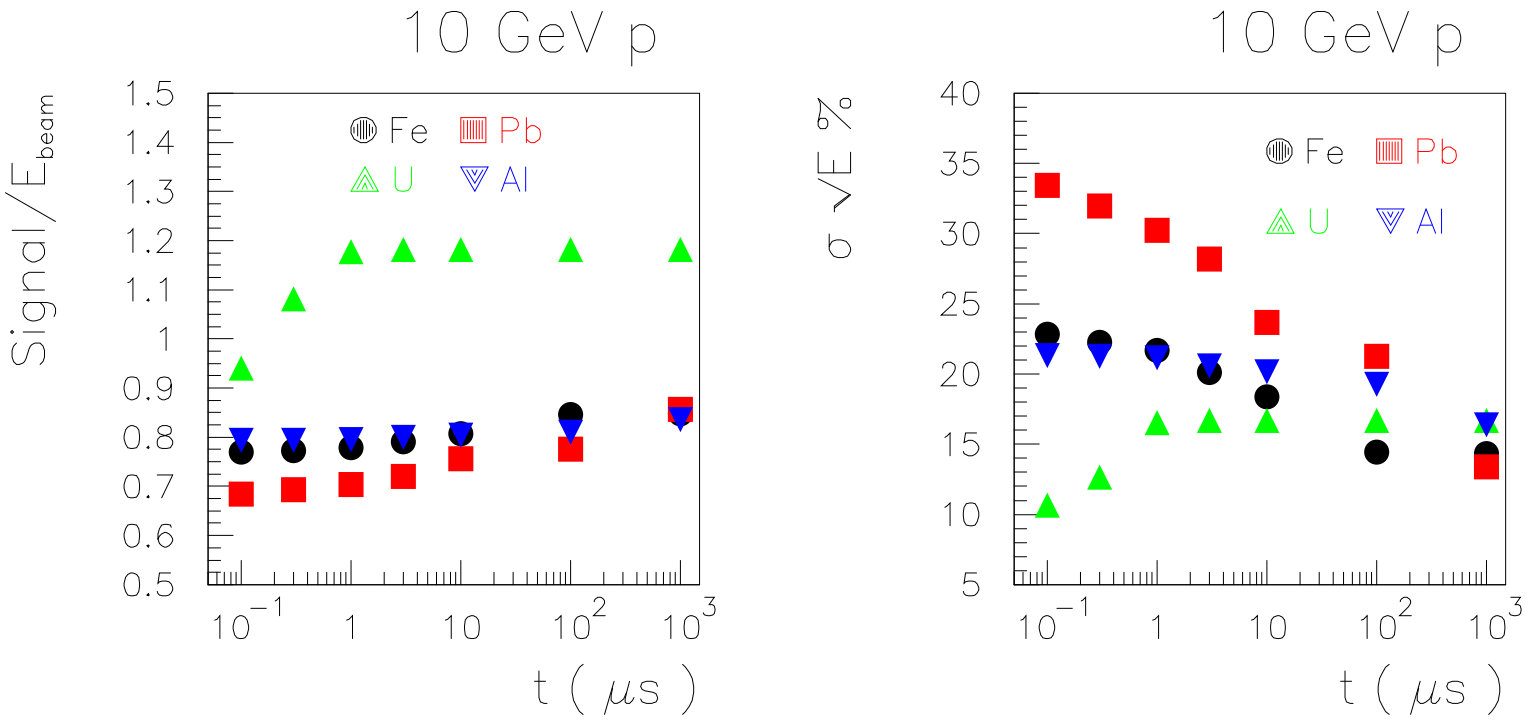

Average "visible" signal (left) (heavy recoil excluded, no quenching) and fractional resolution (right) as a function of integration time. *The time scales are meaningful only for the given materials, hydrogen content could significantly affect neutron thermalization times*

Infinite calorimeters: slow neutrons V

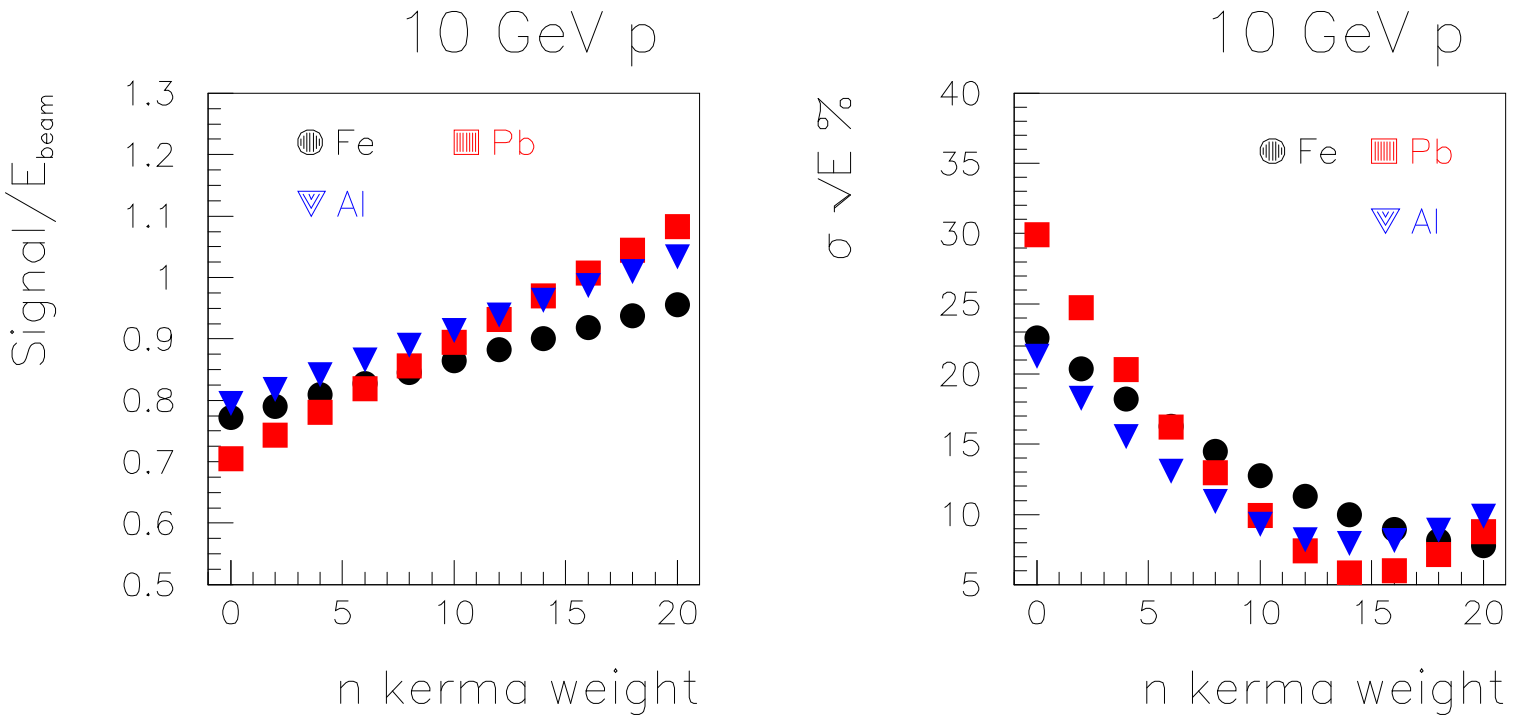

Average "visible" signal (left) (heavy recoil excluded, 30% of neutron produced γ's, no quenching) and fractional resolution (right) as a function of the enhancement of the slow neutron kinetic energy signal (i.e. using hydrogen in the sensitive medium)

Useful references

1. INC: R. Serber, *Phys. Rev.* 72, 1114 (1947); M.L. Goldberger, *Phys. Rev.* 74, 1269 (1948); N. Metropolis et al., *Phys. Rev.* 100, 185 (1958); N. Metropolis et al., *Phys. Rev.* 100), 204 (1958); H.W. Bertini, *Phys. Rev.* 131, 1801 (1963); H.W. Bertini, *Phys. Rev.* C1), 1801 (1970); V.S. Barashenkov et al., *Sov. Phys. Usp.* 16, 31 (1973)

2. Preequilibrium: R. Bonetti, A.J. Koning, J.M. Akkermans, and P.E. Hodgson, *Phys. Rep.* 247, 1 (1994); E. Gadioli, and P.E. Hodgson, *Pre-equilibrium Nuclear Reactions*, (Clarendon Press, Oxford, 1992); M. Blann, Proc. of the *Workshop in Computation and Analysis of Nuclear Reaction Data Relevant to Nuclear Energy and Safety*, Trüste, 1992, (M.K. Mehta and J.J. Schmidt eds., World Scientific, Singapore 1993) 517

3. hN General: C.J. Joachain, *Quantum Collision Theory* (North-Holland, Amsterdam 1975); J.Bystricky et al., DPhPE 87-03 (1987); B.J. VerWest, and R.A. Arndt, *Phys. Rev.* C25, 1979 (1982)

4. General: K. Kikuchi and M. Kawai, *Nuclear Matter and Nuclear Interactions*, (North-Holland, Amsterdam, 1968); A. Bohr, B.R. Mottelson, *Nuclear Structure* Vol. 1, (W.A. Benjamin, Inc. 1969); A. deShalit and H. Feshbach *Theoretical Nuclear Physics, Vol. 1: Nuclear Structure*, (Wiley 1974)

Useful references

5. DPM/QGSM: A. Capella, U. Sukhatme, and J. Tran Thanh Van, *Z. Phys.* C3, 329 (1980); A. Capella, and J. Tran Thanh Van, *Phys. Lett.* B93, 146 (1980); A. Capella et al., *Phys. Rep.* 236, 225 (1994); A. Kaidalov, *Phys. Lett.* B117, 459 (1982); A. Kaidalov, and K.A. Ter-Martirosyan, *Phys. Lett.* B117, 247 (1982); F.W. Bopp, R. Engel, D. Pertermann, and J. Ranft, *Phys. Rev.* D49, 3236 (1994) J. Ranft, *Phys. Rev.* D51, 64 (1995)

6. Evaporation: V.F. Weisskopf, *Phys. Rev.* 52, 295 (1937); N. Bohr and J.A. Wheeler, *Phys. Rev.* 56, 426 (1939) I. Dostrowsky, Z. Fraenkel and G. Friedlander, *Phys. Rev.* 116, 683 (1959); A.S. Iljinov and M.V. Mebel, *Nucl. Phys.* A543, 517 (1992)

7. Glauber: R.J. Glauber, in *Lectures in Theoretical Physics*, Vol. 1 (1959); R.J. Glauber and G. Matthiae, *Nucl. Phys.* B21, 135 (1970), V.N. Gribov, *Sov. Phys. JETP* 29, 483 (1969); V.N. Gribov, *Sov. Phys. JETP* 30, 709 (1970)

8. Modern codes: R. E. Prael and H. Lichtenstein, LA-UR-89-3014 Los Alamos (1989) H.-J. Möring, J. Ranft, *Z. Phys.* C52, 643 (1991); J. Aichelin, *Phys. Rep.* 202, 233 (1991); S.G Mashnik and S.A. Smolyansky, JINR preprint E2-94-353 , Dubna (1994); K. Niita et al., *Phys. Rev.* C52, 2620 (1995); A. Ferrari, P.R. Sala, J. Ranft, and S. Roesler, *Z. Phys.* C70, 413 (1996); A. Ferrari, and P.R. Sala, ICTP Miramare-Trieste, Italy, 15 April–17 May 1996, Proceedings published by World Scientific, A. Gandini, G. Reffo eds, Vol. 2, 424 (1998)

Dual Parton Model: introduction

Dual Parton Model (DPM): originally developed in Orsay in 1979. Together with similar models, i.e. the Quark Gluon String Model (QGSM) developed independently in Russia, it provides a framework for the description of the soft component of high energy hadronic interactions

Recently these models have been extended to include in a coherent approach the hard component as predicted by perturbative QCD.

DPM, QGSM and similar approaches are the theoretical framework adopted by the vast majority of models/codes describing hadronic interactions at accelerator and cosmic ray energies in the 80's and in the 90's

DPM is the framework of choice for the model developed for FLUKA in order to describe hadron-nucleon interaction from several GeV onwards

DPM: generalities

- Problem: the features of "soft" interactions (low-p_T interactions) cannot be derived from the QCD Lagrangian, because the large value taken by the running coupling constant prevents the use of perturbation theory.
- QCD: gluons are coloured $\rightarrow$ strongly self-interacting. Suppose quarks are held together by color lines of force, the gluon-gluon interaction will pull them together into the form of a tube or a string. Since quarks are confined, the energy required to "stretch" such a string is increasingly large until it suffices to materialize a quark-antiquark couple from the vacuum and the string breaks into two shorter ones, with still quarks at both ends.
- Hence because of quark confinement, theories based on interacting strings are powerful tools in understanding QCD at the soft hadronic scale, that is in the non-perturbative regime.
- An interacting string theory naturally leads to a topological expansion. At high energies, such an expansion was developed already before the establishment of QCD, $\rightarrow$ the Reggeon-Pomeron calculus in the framework of perturbative Reggeon Field Theory.

The Dual Parton Model is built introducing partonic ideas into a topological expansion which explicitly incorporates the constraints of duality and unitarity, typical of Regge's theory.

DPM: generalities cont.

DPM: hadron considered as open strings with quarks, antiquarks or diquarks sitting at the ends

- mesons (colorless combination of a quark and an antiquark $q\bar{q}$): strings with their valence quark and antiquark at the ends.
- (Anti)baryons (colorless combinations of three (anti)quarks, qqq): open strings with a (anti)quark and a (anti)diquark at the ends.
- At sufficiently high energies the leading term corresponds to a Pomeron (IP) exchange (a closed string exchange), which has a cylinder topology.
- When an unitarity cut is applied to the cylindrical Pomeron two hadronic chains are left as the sources of particle production.
- While the partons out of which chains are stretched carry a net color, the chains themselves are built in such a way to carry no net color, or to be more exact to constitute color singlets like all naturally occuring hadrons.

In practice, as a consequence of color exchange in the interaction, each colliding hadron splits into two colored system, one carrying color charge c and the other $\bar{c}$. These two systems carry together the whole momentum of the hadron. The system with color charge c ($\bar{c}$) of one hadron combines with the system of complementary color of the other hadron, in such a way to form two color neutral chains. These chains appear as two back-to-back jets in their own centre-of-mass systems.

DPM: chain building

The exact way of building up these chains depends on the nature of the projectile-target combination (baryon-baryon, meson-baryon, antibaryon-baryon, meson-meson):

Let be $q_p^v(\bar{q}_p^v)$ the valence (anti)quarks of the projectile, and with q_t^v those of the target, and assume that the (anti)quarks sitting at one end of the baryon strings carry momentum fraction x_p^v and x_t^v respectively

- baryon-baryon scattering chains: $q_t^v - q_p^v q_p^v$ and $q_p^v - q_t^v q_t^v$
- meson-baryon scattering chains: $q_t^v - \bar{q}_p^v$ and $q_p^v - q_t^v q_t^v$
- antibaryon-baryon scattering chains: $q_t^v - \bar{q}_p^v$ and $\bar{q}_p^v \bar{q}_p^v - q_t^v q_t^v$

DPM: chain examples

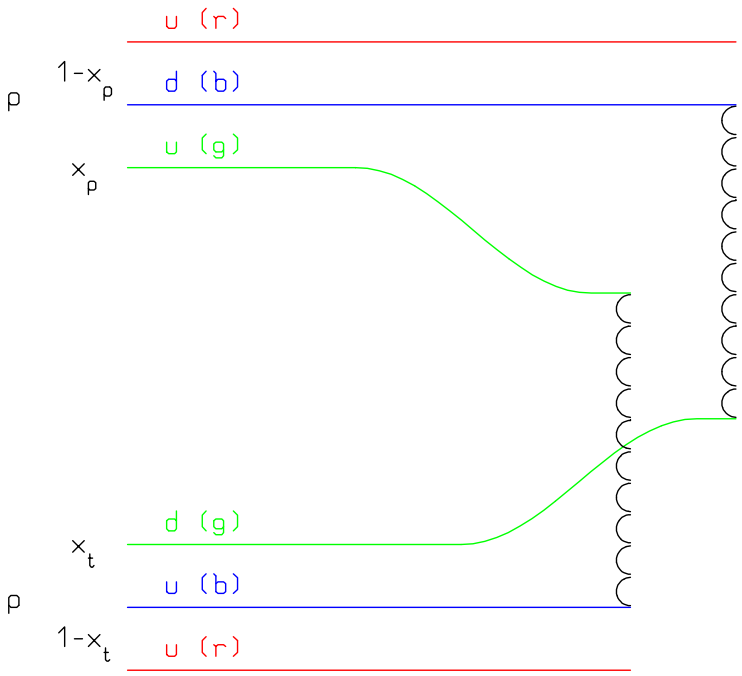

Leading two-chain diagram in DPM for $p-p$ scattering. The color (red, blue, and green) and quark combination shown in the figure is just one of the allowed possibilities

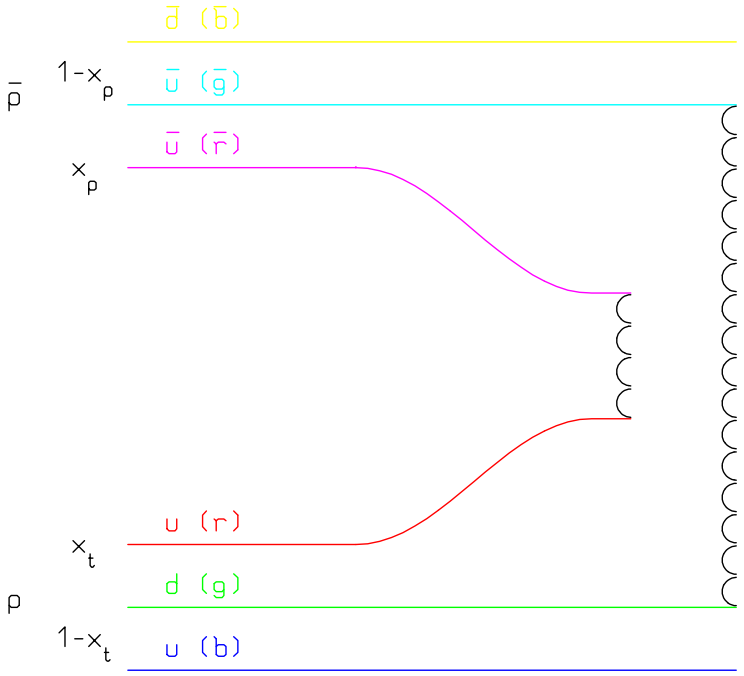

Leading two-chain diagram in DPM for $\bar{p}-p$ scattering. The color (red, blue, and green) and quark combination shown in the figure is just one of the allowed possibilities

DPM: chain examples II

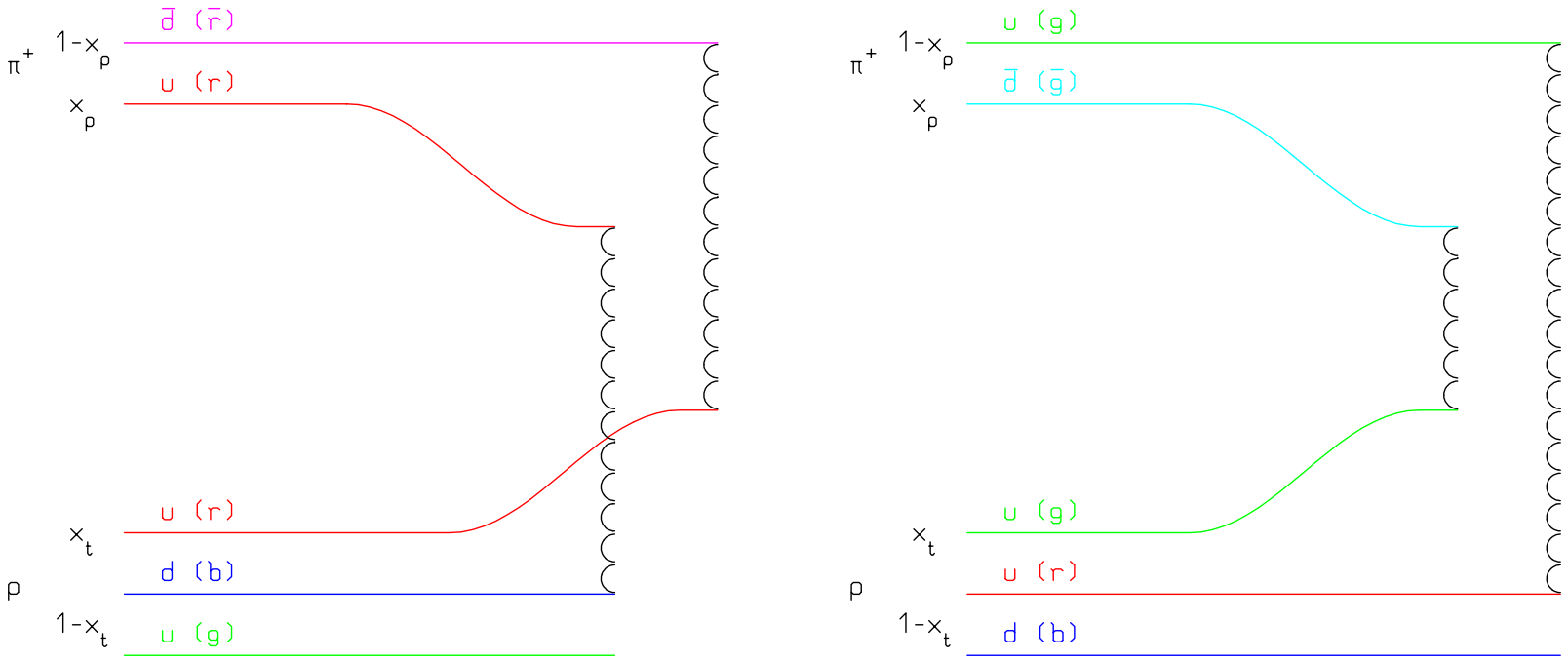

Leading two-chain diagrams in DPM for $\pi^+ - p$ scattering. The color (red, blue, and green) and quark combination shown in each figure is just one of the allowed possibilities

DPM: chain energies and momenta

The energy and momentum in the centre-of-mass system of the collision, as well as the invariant mass squared of the two chains, are given by:

$$
\begin{aligned}
E^*_{ch1} &\approx \frac{\sqrt{s}}{2}(1 - x^v_p + x^v_t) \\
E^*_{ch2} &\approx \frac{\sqrt{s}}{2}(1 - x^v_t + x^v_p) \\
p^*_{ch1} &\approx \frac{\sqrt{s}}{2}(1 - x^v_p - x^v_t) = -p^*_{ch2} \\
s_{ch1} &\approx s(1 - x^v_p)x^v_t \\
s_{ch2} &\approx s(1 - x^v_t)x^v_p
\end{aligned}
$$

DPM: multiple soft chains

The single Pomeron exchange diagram is the dominant contribution, however higher order contributions with multi-Pomeron exchanges become important at energies in excess of 1 TeV in the laboratory

They correspond to more complicated topologies, and DPM provides a way for evaluating the weight of each, keeping into account the unitarity constraint

When cut, every extra Pomeron exchanged gives rise to two extra chains which are built using two $q\bar{q}$ couples excited from the projectile and target hadron sea respectively.

The inclusion of these higher order diagrams is usually referred to as *multiple soft collisions*.

DPM: momentum distributions

The exact form of the momentum distribution for the x variables of valence and sea quarks, $P(x_1, .., x_n)$, is unknown.

However, general considerations based on Regge arguments allow to predict the asymptotic behaviour whenever each of its arguments goes to zero.
The behaviour turns out to be singular in all cases, but for the diquarks.

A reasonable assumption is therefore to approximate the true unknown distribution function with the product of all these asymptotic behaviours, treating all the rest as a normalization constant

DPM: momentum distributions II

Under this approximation, indicating with $x_{q\ i}^{sea}$, and $x_{\bar{q}\ i}^{sea}$, the energy/momentum fractions carried by the sea quarks and with X_i^{sea} the sum of $x_{q\ i}^{sea}$ and $x_{\bar{q}\ i}^{sea}$, the total momentum distribution function for a(n) (anti)baryon in the case of $n_{I\!P}$-cut Pomerons can be written as:

$$\begin{aligned} P(\bar{x})\mathrm{d}\bar{x} &\approx C_b\ x_q^{-\frac{1}{2}} x_{qq}^{\frac{3}{2}} \prod_i^{n_{I\!P}-1} (X_i^{sea})^{-1} (x_{q\ i}^{sea})^{-\frac{1}{2}} (x_{\bar{q}\ i}^{sea})^{-\frac{1}{2}} \\ &\cdot \ \delta(1 - x_q - x_{qq} - \sum_i^{n_{I\!P}-1} X_i^{sea})\ \mathrm{d}\bar{x} \qquad (3) \\ \bar{x} &\equiv x_q \cdot x_{qq} \prod_i^{n_{I\!P}-1} \left(x_{\bar{q}\ i}^{sea} \cdot x_{q\ i}^{sea}\right) \end{aligned}$$

where C_b is a normalization factor. The momentum distribution function for a meson reads:

$$\begin{aligned} P(\bar{x})\mathrm{d}\bar{x} &\approx C_m\ x_q^{-\frac{1}{2}} x_{\bar{q}}^{-\frac{1}{2}} \prod_i^{n_{I\!P}-1} (X_i^{sea})^{-1} (x_{q\ i}^{sea})^{-\frac{1}{2}} (x_{\bar{q}\ i}^{sea})^{-\frac{1}{2}} \\ &\cdot \ \delta(1 - x_q - x_{\bar{q}} - \sum_i^{n_{I\!P}-1} X_i^{sea})\ \mathrm{d}\bar{x} \\ \bar{x} &\equiv x_q \cdot x_{\bar{q}} \prod_i^{n_{I\!P}-1} \left(x_{\bar{q}\ i}^{sea} \cdot x_{q\ i}^{sea}\right) \end{aligned}$$

Chain hadronization

The latter ingredient is a *hadronization model*, which must take care of transforming each chain into a sequence of physical hadrons, stable ones or resonances

The basic assumption is that of *chain universality*, which assumes that once the chain ends and the invariant mass of the chain are given, the hadronization properties are the same regardless of the physical process which originated the chain

Therefore the knowledge coming from hard processes and e^+e^- collisions about hadronization can be used to fulfill this task. There are many more or less phenomenological models which have been developed to describe hadronization. In principle hadronization properties too can be derived from Regge formalism

DPM: summary

Summarizing, DPM provides recipes for performing the following tasks:

- determining the number of cut Pomerons, and therefore the number of chains contributing to the reaction
- forming the chains using the valence and possibly sea quarks of the two colliding hadrons
- determining the energy and momentum carried by each chain, according to the momentum distribution functions of the two colliding hadrons
- hadronizing each chain producing the final hadrons, stable ones or resonances

The last step is not exactly a part of DPM, but rather DPM is factorized in such a way that it can be accomplished using whichever hadronization scheme. In principle there is little or no freedom in each individual step, therefore strenghtening the predictive power of the model
Actually, in the energy range of interest for experiments, threshold effects are still very important. While DPM is assumed to be valid in the asymptotic regime, and treats massless partons at energies large enough to neglect hadron masses,most practical implementations deal with chains with invariant masses so small that only few particles can be produced out of the chain itself

It is possible to extend DPM to hadron-nucleus collisions making use of the Glauber-Gribov approach. Furthermore DPM provides a theoretical framework for describing hadron diffractive scattering both in hadron-hadron and hadron-nucleus collisions.